Dynamic Modeling and Multivariable Control of Vapor Compression Cycles in Air Conditioning Systems

by

Xiang-Dong He

B.S. in Applied Mechanics
Zhejiang University, China, 1985

M.S. in Applied Mechanics
Beijing University, China, 1988

Submitted to the Department of Mechanical Engineering in Partial Fulfillment of the Requirements for the Degree of

DOCTOR OF PHILOSOPHY

at the

MASSACHUSETTS INSTITUTE OF TECHNOLOGY

February 1996

Signature of Author _____
Department of Mechanical Engineering
January 10, 1996

Certified by _____
Haruhiko H. Asada, Professor of Mechanical Engineering
Thesis Supervisor

Certified by _____
Sheng Liu, Research Scientist of Mechanical Engineering
Thesis Co-supervisor

Accepted by _____
Ain A. Sonin
Chairman, Department Committee on Graduate Students

Dynamic Modeling and Multivariable Control of Vapor Compression Cycles in Air Conditioning Systems

Xiang-Dong He

Submitted to the Department of Mechanical Engineering
on January 10, 1996
in partial fulfillment of the requirements
for the Degree of Doctor of Philosophy

Abstract

Driven by strong market competition, the performance of air conditioning systems has improved in numerous ways over the years. However, the fundamental control methodology that operates the underlying vapor compression cycle remains rudimentary: the room air temperature is regulated by compressor capacity control while the system superheat is controlled by an expansion device. The performance of these decoupled single-input single-output (SISO) feedback loops is inherently limited in terms of transient behavior and energy efficiency, due to the strong cross-coupling among feedback loops. This thesis presents a systematic control design method based on effective modeling and modern multivariable feedback techniques to coordinate control efforts, such as compressor speed and expansion valve opening, in order to achieve greater improvement over conventional schemes.

To develop an effective model for the purpose of control design, a moving-interface lumped parameter model is first developed to describe the dynamics of two-phase flow heat exchangers. A low order, compact dynamic model of the vapor compression cycle is established by integrating heat exchanger models with simplified models of the compressor and the expansion valve under appropriate connecting conditions. The resultant model is simple and yet effective enough in reflecting the main dynamic characteristics of a vapor compression cycle, and is readily applicable to feedback control design. This model is validated by extensive experimental tests.

To synthesize a model-based multivariable control system, the LQG technique is applied with guaranteed stability robustness in the design. Furthermore, to control a vapor compression cycle over a wide range where system nonlinearities become evident, the multivariable controller is designed to adapt to changing operating conditions based on a gain scheduling scheme. Both analytical studies and experimental tests show that the multivariable control can significantly improve the transient behavior of vapor compression cycles compared to the conventional SISO control scheme.

Thesis Supervisor: Haruhiko H. Asada
Title: Professor of Mechanical Engineering

Thesis Co-supervisor: Sheng Liu
Title: Research Scientist of Mechanical Engineering

Dedicated to my parents

Acknowledgments

I would like to take this opportunity to express my sincere thanks to my thesis supervisor, Professor Haruhiko H. Asada, for his inspiring guidance and constant encouragement. I benefited greatly from his profound vision, keen insight, and his constant efforts to provide the leadership in new research directions. I also wish to thank Mrs. Kumiko Asada for her nice consideration and kindness during my years at MIT. I wish to express my great gratitude to my thesis co-supervisor, Dr. Sheng Liu, for his sound advice, valuable support and warm friendship. I really benefited a lot while working with him.

My thesis committee members, Professor Anuradha M. Annaswamy and Professor Peter Griffith have also made valuable contributions to the direction and quality of this thesis work. I would like to thank them for many helpful advice and suggestions.

I express my deep gratitude to my sponsor, Daikin Industries Ltd, for their support. I would like to thank Dr. Torikoshi, Mr. Shimadzu, Mr. Yonemoto, Mr. Hori, Mr. H. Itoh, Mr. T. Hiei, Mr. K. Nakagawa, Mr. S. Sakamoto, Mr. Yamashita, and Ms. Tsuji for their support and valuable helps. Especially, I wish to thank Mr. Itoh for his constant support, inspiring advice, and encouragement. From him, I learn to see things with a deep vision and work effectively in a team. During my visits to Daikin in 1995, I had the pleasure of working directly with Mr. Nakagawa and Mr. Sakamoto. They made valuable contributions to the experimental work in this thesis.

I would like to thank all of my colleagues in the Intelligent Machines Laboratory. Without the help and friendship from the lab group, the work and life at MIT would not have been so beneficial and enjoyable. Especially, I would like to thank Booho Yang, Sean Li, Ming Zhou, Anton Pil, Samir Nayfeh, Danny Braunstein, Jahng Park, Sooyong Lee, Susan Ipri, Mark West, and Atushi Toizumi.

I am grateful to Dr. Cliff Federspiel for his valuable helps at the early stage of this thesis. I am greatly indebted to Dr. Charlie Culp for his support, understanding and generosity.

I wish to thank Dr. Doyne Farmer, Dr. Alan Lapades, Dr. James Theiler at Los Alamos National Laboratory, under their advice and guidance I spent extremely useful one year and two summers doing research there.

To my close friends, Jingfeng Wang, Xiaoming Zhang, Qing Zhou, Qing Wang, and many others, I want to thank you for much needed support, life advice, or dinner companionship.

I would like to express my sincere appreciation to Professor Decheng Chen, Professor Zhaoxuan Zhu, and Dr. Shiyi Chen for their constant moral support over the years.

Finally, to my dear fiancée Lei Yan, I wish to express the deepest thanks for your love, support and friendship.

Contents

1 Introduction **10**

1.1 Background and Objectives 10

1.2 Previous Works 13

2 Dynamics of Two-Phase Flow Heat Exchangers **16**

2.1 Introduction 16

2.2 One-Dimensional Thermofluid Continuous Models 19

2.3 A Moving-Interface Lumped-Parameter Model 21

2.4 Model Linearization 26

3 Dynamic Model of a Vapor Compression Cycle **28**

3.1 Introduction 28

3.2 Models of other main components 30

3.2.1 A Lumped-Parameter Model for Condenser Dynamics 30

3.2.2 Models of Expansion Valves and Compressors 35

3.3 Model of a whole vapor compression cycle 39

3.4 Model Linearization 43

3.5 Validation of the Linearized Model 47

3.5.1 Experimental Set-up 47

3.5.2 Parameter Estimation 50

3.5.3 Simulation of the Model and Comparisons to Experimental Results 57

3.6 A simplified model 63

4 Multivariable Control of Vapor Compression Cycles **65**

4.1 Introduction 65

4.2 Analysis of traditional control scheme in air conditioning systems . . . 67

4.3 Model-based MIMO control of vapor compression cycles 71

4.3.1 A multivariable control design method: LQG with integrator . . 71

4.3.2 Digital implcmentation and Experimental results 75

4.3.3 Control of vapor compression cycle over a wide range using gain scheduling scheme 80

5 Conclusions **84**

5.1 Thesis Summary 84

5.2 Main Impacts on HVAC&R Systems 85

References **88**

Appendix A **92**

Appendix B **93**

Appendix C **94**

Appendix D **95**

List of Figures

2.1 A schematic of a vapor compression cycle. 17

2.2 Illustration of time-invariant mean void fraction. 18

2.3 A schematic of an evaporator model. 22

3.1 A schematic of vapor compression cycle model. 29

3.2 A schematic of a condenser model. 31

3.3 Schematic of a simple reciprocating compressor. 38

3.4 Pressure-enthalpy diagram of compressor. 39

3.5 Experimental Setup 48

3.6 A schematic of the test room 49

3.7 Step responses under a step change in compressor speed. 58

3.8 Step responses under a step change in expansion valve opening. 59

3.9 Step responses under a step increase of heat transfer coefficient α_o at the indoor unit side 60

3.10 Step responses under a step change of heat transfer coefficient α_o at the outdoor unit side 60

3.11 Simulated results and actual system response measured from experiments. The compressor speed is changed from 70Hz to 75Hz 61

3.12 Simulated results and Actual system response measured from experiments. The expansion valve opening has 10 steps increase 62

3.13 A 5-th order lumped-parameter model 64

4.1 A decouple SISO control system 68

4.2 Root locus of the transfer function from a_v to SH (partially shown here) 68

4.3 Valve-controlled SH response to a step change in compressor speed. . . 69
4.4 Compressor-controlled P_e response to a step change in valve opening. . 69
4.5 A decouple SISO control system 70
4.6 Performance of a SISO control system 70
4.7 A multivariable control system 72
4.8 A block diagram of LQG 72
4.9 A block diagram of LQG with integrators 74
4.10 Frequency domain singular values 76
4.11 Command following: Desired Te has a step change 77
4.12 Command following: Desired superheat has a step change 78
4.13 Disturbance rejection: indoor fan speed changed from 1000rpm to 1200rpm 79
4.14 Effect of high control gain 80
4.15 A schematic of gain schedule 81
4.16 Control of vapor compression cycle in a wide range 82
4.17 COP and cooling capacity of the MIMO control and the SISO control . 83

Chapter 1
Introduction

1.1 Background and Objectives

Vapor compression cycles are widely used for industrial and residential applications, such as heat pumps and air conditioning systems. Modeling, control, and diagnostics of vapor compression cycles have been active research subjects for years for improving energy efficiency. Most of these research works are concerned with the steady-state operation of such systems, despite the fact that steady-state conditions are almost never reached, and the actual coefficient of performance (COP) may be considerably lower than that claimed by the manufacturers.

In a vapor compression cycle, the evaporator and condenser are the two-phase flow heat exchangers that interact with indoor or outdoor air respectively, depending on its heating or cooling application. During the cycle operation, energy efficiency is closely dependent on the thermodynamic states of refrigerant at various components in the cycle loop. In principle, the cycle loop can be characterized by evaporating temperature, condensing temperature, superheat at the evaporator outlet, and subcooling at the condenser outlet. A proper regulation of these state variables and their dynamic behavior can lead to energy-efficient operations; more importantly, it also affects the machine's service life. For instance, superheat regulation is extremely important to the compressor operation. The desired superheat is usually set between $5°C \sim 10°C$. For values below this, there may be the danger of liquid refrigerant entering the compressor. When it is too high, the energy efficiency is low, and the excessively heated vapor may dramatically increase the compressor discharge temperature. In practice,

superheat is often regulated by a thermostatic expansion valve. It is well known that oscillatory behavior or "hunting" often occurs when a thermostatic expansion valve is used. Broersen and van der Jagt reported in [2] that such oscillatory behavior can be attributed to the dynamics of the closed-loop system consisting of the refrigerant flow and the thermostatic valve.

Over the years, heat pumps and air conditioners have been operated in a cyclic on-off manner for temperature regulation. It is well known that frequent start-up and shut-down transients entailed in the on-off control result in poor energy efficiency. The introduction of variable speed compressors to the vapor-compression cycle has greatly improved its operation flexibility. The compressor speed can be continually adjusted so as to modulate the heat exchanger capacity for matching the actual loading condition. Therefore, the discontinuous on-off operation can be avoided and the energy efficiency can be improved. This is generally known as capacity control [15].

In addition to variable-speed compressors, adjustable expansion valves and variable-speed fans are also available now in heat pumps and air conditioning systems. The opening of an expansion valve can affect refrigerant flow rate as well as pressure drop between the condenser and evaporator, which not only can change the overall COP, but also has a direct influence on the superheat at the evaporator outlet. The influence of fan speeds on the two heat exchangers is in the heat transfer coefficient between air and heat exchanger wall. By changing the fan speeds, heat transfer rate can be altered, which results in variations in COP, evaporating pressure, condensing pressure, superheat, as well as subcool.

These variable-speed drives offer opportunities of improving both energy efficiency and machine operation reliability. However, before one can take full advantage of these actuating inputs to operate a vapor compression cycle, the role of each actuator

in affecting the overall cycle behavior, including at transients and steady states, must be clarified. In particular, how to combine and coordinate these various inputs so as to achieve multiple task goals such as capacity modulation and superheat regulation is a key issue to be addressed. To this end, a sound understanding of the physical behavior of a vapor compression cycle is indispensable. One of main objectives of this thesis is aimed at developing and validating an effective model of vapor compression cycle dynamics for the purpose of designing advanced control and diagnostic schemes that are readily applicable to commercial heat pumps and air conditioning systems.

To be incorporated into a real-time control design, a model must be expressed in an explicit form of input-output relation. For the case of vapor compression cycle, the actuating inputs and performance outputs are involved in a set of high-order, nonlinearly coupled equations, due to the distributed, two-phase nature in this thermo-fluid system. The thesis derives and validates a model with the simplicity of a lumped-parameter model while preserving a faithful representation of compression cycle dynamics. In particular, performance outputs such as evaporating and condensing pressures, superheat, will be expressed explicitly in a canonical state space form as functions of actuating inputs. To this end, at first, the set of partial differential equations that govern general thermo-fluid systems are converted into ordinary differential equations, based on a concept of transition point in two-phase flow heat exchangers. The resultant lumped-parameter model is then analyzed by studying the cycle dynamics in the vicinity of a certain normal operating point, the so called "short transients" in related literature, as opposed to the "long transients" during start-up and shut-down phases. Short transients are studied based on the linearized model, which provides insight into the energy exchange mechanism in a vapor compression cycle as well as how this mechanism can be perturbed by small changes in actuating inputs.

The derivation of this dynamic model is also based on the moving-boundary approach, as described in [9]. The main difference is in the modeling of the tube wall temperature, which is also simplified in this model to a multi-node form with boundaries coincide with the moving interfaces. The analytic model is carefully validated through experiments by estimating all parameters involved, simulation and comparisons. The model can be further simplified to reflect the low-order dynamic behavior of vapor compression cycle. The resultant simplicity and validity of this model make it well suited for model-based control system synthesis.

The second main objective of this thesis is to develop a multivariable control system to regulate vapor compression cycles based on the dynamic model. This thesis investigates the limitation of the conventional single-input single-output(SISO) control scheme in air conditioning systems, and presents theory and experimental results of model-based multivariable controls for improving the transient responses of vapor compression cycles.

This thesis is organized as follows. In chapter 2, the moving-interface lumped parameter model is presented to describe the dynamics of two-flow heat exchangers. In chapter 3, the analytic model of vapor compression cycles is proposed, followed by the experimental estimation of parameters involved in the model, and simulation and validation of the model through experimental tests. Multivariable control for vapor compression cycle is presented in chapter 4. Concluding remarks are given in chapter 5.

1.2 Previous Works

Published literature in dynamic modeling of vapor compression cycle and control of air conditioning systems have been studied. Several works have been done on

modeling the dynamics of a vapor compression cycle. In most of these works, spatial dependency was ignored. These include the single-node, lumped-parameter models in [3], [27], and [5]. While these lumped-parameter models are quite useful for predicting the response of *average* refrigerant properties in heat exchangers, they fail to reflect critical properties such as refrigerant superheat or subcooling values, which can only be captured through a spatial distribution analysis. MacArthur and Grald [21] presented a unsteady compressible two-phase model for predicting heat pump performance based on partial differential equations that govern the transient and transport of thermofluid properties. This model is a useful tool for simulating the dynamic response of the refrigeration system and its spatial distribution with a high accuracy. However, it is by far too complex to be used for any control design purpose.

They presented in [9] a moving-boundary approach in order to reduce the computation complexity relatively to the spatially distributed approach. This moving-boundary formulation was based on the transition point concept first described by [29]. The spatial dependence of the heat exchanger was approximated by converting the governing partial differential equations into ordinary differential equations. Although the computation of two-phase refrigerant dynamics was greatly simplified in [9], the response of tube wall temperature was still modeled based on the spatial dependent approach. Hence, the overall computation load is still too complex to be applied to any control design.

There have been lots of research works on the control of air conditioning systems. On-off control was introduced initially for operating an air conditioning machine. Compressor capacity control was investigated when the inverter technology was not fully developed [15]. The approach was based on the single-input single-output(SISO) methodology. Many researches proposed different SISO PID controllers

for compressor speed and expansion valve opening since electronic expansion valve was invented and variable-speed compressors were available. In [20], an optimal control method was proposed by using variable-speed compressor and indoor fan flow rate. Miller did an experimental research on the optimal control of air conditioning systems equipped with variable speed compressor and indoor fan speed [23]. However, all these research works discussed empirical steady state open loop controls. This thesis is the first attempt to develop closed loop feedback multivariable control system based on a vapor compression cycle model.

Chapter 2
Dynamics of Two-Phase Flow Heat Exchangers

2.1 Introduction

Two-phase flow heat exchangers have been widely used in vapor-compression cycles for industrial and residential applications, such as heat pumps, air conditioning systems, and refrigeration systems. Figure 2.1 depicts a schematic of a vapor compression cycle, where the evaporator and condenser are the two-phase flow heat exchangers that interact with indoor or outdoor air respectively, depending on its heating or cooling application. In the cooling mode, the indoor heat exchanger is an evaporator. High quality two-phase flow of refrigerant enters the evaporator, evaporates along the heat exchanger tubes, and becomes the superheated vapor at the exit of evaporator. During the evaporating process, the liquid in the two-phase flow is gradually changed into vapor, and the heat is absorbed from the indoor air to realize the phase change of the liquid refrigerant. Most of analysis of heat exchangers are concerned with the steady-state operation of such systems, however steady-state conditions are almost never reached, and the dynamics of heat exchangers is of importance to the system performance.

Several works have been done on modeling the dynamics of two-phase flow heat exchangers. Most of these works employed a simplified heat exchanger model in which spatial dependency was ignored. These include the single-node, lumped-parameter models in [3], [5], and [27]. In [28], a three-lump model of a two-phase flow heat exchanger was established based on a temperature-entropy bond graph. While these lumped-parameter models are quite useful for predicting the response of *average* refrig-

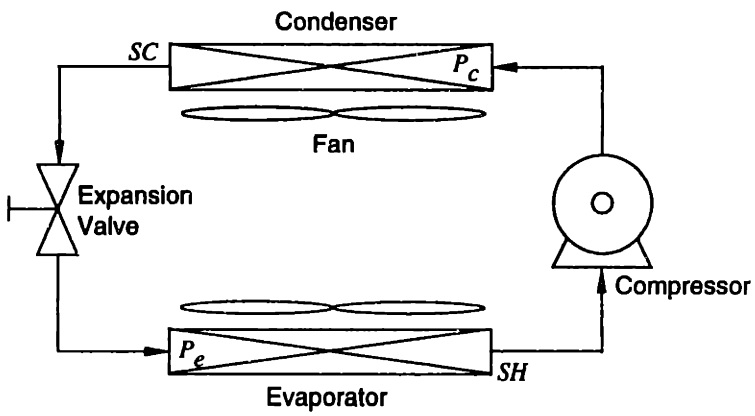

Figure 2.1: A schematic of a vapor compression cycle.

erant properties in heat exchangers, they cannot reflect explicitly critical properties such as refrigerant superheat or subcool value, which can only be captured through a spatial distribution analysis. MacArthur and Grald [21] presented a unsteady compressible two-phase model for predicting heat pump performance based on partial differential equations that govern the transient and transport of thermofluid properties. This model is a powerful tool for simulating the dynamic response of refrigerant properties and their spatial distribution. Compared with experimental data, the prediction from this model was quite accurate. However, this model requires iterations at each time step to solve the high-order, nonlinear simultaneous equations for all state variables. No explicit input-output equations are available and readily applicable to control design.

Wedekind's work in [30] is critically important in simplifying a class of two-phase transient flow problems into the type of lumped-parameter systems. With experimental confirmation, Wedekind showed that the mean void fraction (the volumetric ratio of vapor to liquid) remains relatively invariant in the two-phase region of a heat ex-

changer during most operations. This implies that under different inflow conditions, the liquid dry out point in an evaporator, for example, may change its location along the evaporator tube; however, the distribution of liquid/vapor remains similar at all time. This similarity property enables us to characterize the liquid/vapor distribution in the two-phase region by a single variable, i.e. the mean void fraction, denoted $\bar{\gamma}$. This concept is depicted in Figure 2.2 where $l_e(t)$ is the location of the liquid dry-out point in an evaporator measured from the inlet. Mean void fractions in two instants, denoted $\gamma(t_1)$ and $\gamma(t_2)$, remain similar, even though $l_e(t_1)$ and $l_e(t_2)$ are different due to changes in inflow conditions.

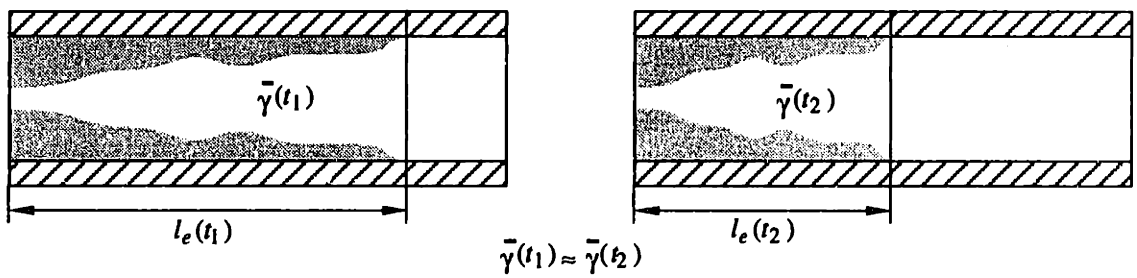

Figure 2.2: Illustration of time-invariant mean void fraction.

In this chapter, based on the principle of time-invariant mean void fraction, the spatial dependence of heat exchangers was approximated by converting the governing partial differential equations into ordinary differential equations. As a result, the dynamic behavior of superheat and subcool can be captured. Similar works have been done by [2], [10], and [9]. However, they all require complex numerical procedures for accurate simulations, not suitable for model-based control design.

2.2 One-Dimensional Thermofluid Continuous Models

Based on the conservation principles of mass, momentum, and energy, the dynamics of two-phase flow heat exchangers can be described mathematically by a set of complex, coupled, nonlinear partial differential equations. Several assumptions must be made in order to simplify these equations into a mathematically tractable form. These assumptions include (1) the heat exchanger is a long, thin, horizontal tube; (2) the refrigerant flowing through the heat exchanger tube can be modeled as a one-dimensional fluid flow; (3) axial conduction of refrigerant is negligible.

The one-dimensional partial differential equations that govern the conservation of mass, momentum, and energy of refrigerant flowing through a heat exchanger tube can be written as:

$$\text{Mass balance:} \quad \frac{\partial \rho}{\partial t} + \frac{\partial (\rho u)}{\partial z} = 0 \tag{2.1}$$

$$\text{Momentum balance:} \quad \frac{\partial (\rho u)}{\partial t} + \frac{\partial (\rho u^2 + P)}{\partial z} = -\frac{4}{D_i}\lambda \frac{1}{2}\rho u^2 \tag{2.2}$$

$$\text{Energy balance:} \quad \frac{\partial (\rho h - P)}{\partial t} + \frac{\partial \rho u h}{\partial z} = \frac{4}{D_i}\alpha_i (T_w - T_r) \tag{2.3}$$

where

ρ: density of refrigerant

u: velocity of refrigerant flowing along the tubes

P: pressure of refrigerant

λ: friction coefficient.

D_i: the inner diameter of the tube

h: enthalpy of the refrigerant

T_r: the bulk temperature of the refrigerant

T_w: the temperature of the tube wall

α_i: heat transfer coefficient between the tube wall and the refrigerant per unit area

A detailed derivation of equations (2.1) $\sim$ (2.3) can be found in [21]. The mass flow rate can be shown as $\dot{m} = \rho u A$, where $A = \frac{\pi}{4} D_i^2$. Since the mass flow rate is a variable of interest, and the cross-sectional area, A, is assumed to be constant, equations (2.1) $\sim$ (2.3) can be rewritten as

$$\frac{\partial A\rho}{\partial t} + \frac{\partial \dot{m}}{\partial z} = 0 \tag{2.4}$$

$$\frac{\partial \dot{m}}{\partial t} + \frac{\partial(\frac{\dot{m}^2}{\rho A} + AP)}{\partial z} = -\frac{4}{D_i}\lambda\frac{1}{2}\frac{\dot{m}^2}{\rho A} \tag{2.5}$$

$$\frac{\partial(\rho A h - AP)}{\partial t} + \frac{\partial \dot{m} h}{\partial z} = \pi D_i \alpha_i (T_w - T_r) \tag{2.6}$$

For the heat exchanger tube wall, the energy balance equation can be written as

$$(C_{Pw}\rho_w A_w)\frac{\partial T_w}{\partial t} = \pi D_i \alpha_i (T_r - T_w) + \pi D_o \alpha_o (T_a - T_w) \tag{2.7}$$

where

C_{Pw}: heat capacity of the tube wall

ρ_w: density of the tube wall

A_w: cross-section area of tube wall, $= \frac{\pi}{4}(D_o^2 - D_i^2)$

D_o: outer diameter of the tube

T_a: temperature of the inlet air to the heat exchanger element

α_o: equivalent heat transfer coefficient between the tube wall and the air

Equations (2.4) $\sim$ (2.7) represent a set of coupled equations where a unique solution exists if appropriate initial conditions and boundary conditions are specified. One set of independent state variables can be selected as $P(z,t), h(z,t), \dot{m}(z,t)$ and $T_w(z,t)$, which are functions of both time and spatial coordinates. Other unknown variables

include $\rho(z,t)$ and $T_r(z,t)$. Based on the refrigerant thermodynamics properties, $\rho(z,t)$ and $T_r(z,t)$ can be determined via $\rho(z,t) = \rho(P,h)$ and $T_r(z,t) = T(P,h)$ respectively.

To solve this spatially dependent, unsteady, compressible, two-phase flow problem requires a considerable amount of effort. MacArthur and Grald proposed a method to solve these partial differential equations numerically by discretizing the entire tube into a large number of sections and applying the finite difference technique [21]. MacArthur and Grald's approach is the first one in simulating dynamics of two-phase flow heat exchangers based on a continuous model. Their simulation results were quite accurate when compared to experimental data. However, the computation complexity involved is enormous. And by no means this continuous model can be incorporated into a real-time control system. To meet our control design purpose, we need a heat exchanger model which is simple, mathematically tractable, and yet effective enough in reflecting the essential dynamic characteristics of a heat exchanger. In the following section, a lumped-parameter model is derived by integrating the governing partial differential equations based on the transition point concept discussed in [29]. The resultant model is well suited for feedback control design as well as for transient analysis.

2.3 A Moving-Interface Lumped-Parameter Model

In this section, we focus our attention on deriving a lumped-parameter evaporator model. A lumped-parameter condenser model can be obtained based on the same principles discussed here and will be presented in next chapter. The configuration of the heat exchanger considered here is of the cross-flow type with air as the secondary fluid. By the phase of refrigerant, an evaporator can usually be divided into two parts: a liquid-vapor mixture section and a superheated vapor section, as depicted in Figure 2.3. For a condenser, there is an additional part: the subcooled liquid section.

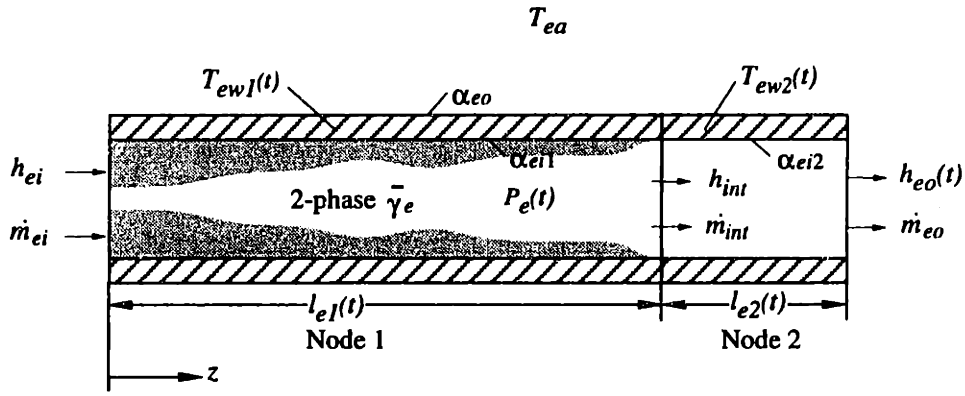

Figure 2.3: A schematic of an evaporator model.

Compared with the total pressure head, the pressure drop along the evaporator tube due to momentum change in refrigerant and viscous friction is negligible. Therefore, refrigerant pressure can be assumed uniform along the entire evaporator tube, and the momentum equation (equation (2.5)) is no longer needed. In the two-phase section, the refrigerant temperature is at its saturated value with no spatial variation. In the superheated section, the temperature of refrigerant increases as it travels from the two-phase/vapor interface toward the evaporator outlet. For this distinction in temperature variation, we lump the evaporate dynamics into two nodes: the two-phase node and the superheated node.

Let us consider mass flow rate at the evaporator inlet $\dot{m}_i$, inflow enthalpy h_i, and mass flow rate at the outlet $\dot{m}_o$ as the boundary conditions for the governing partial differential equations of the evaporator dynamics (subscription e in Figure 2.3 represents evaporator). Let $L_1(t)$ denote the length of the two-phase section measured from the evaporator inlet. Note that $L_1(t)$ varies with time due to any change in boundary conditions. By integrating equation (2.6) from $z = 0$ to $z = L_1(t)$, we

obtain the energy balance equation for node 1 (see appendix for derivation).

$$AL_1\left(\frac{d(\rho_l h_l)}{dt}(1-\bar{\gamma})+\frac{d(\rho_g h_g)}{dt}\bar{\gamma}-\frac{dP}{dt}\right)+A(1-\bar{\gamma})(\rho_l h_l-\rho_g h_g)\frac{dL_1}{dt}=$$
$$\dot{m}_1 h_1-\dot{m}_{int}h_{int}+\alpha_{i1}\pi D_i L_1(T_{w1}-T_{r1}) \tag{2.8}$$

where ρ_l and ρ_g are saturated liquid and vapor densities, respectively, h_l and h_g are saturated liquid and vapor specific enthalpies, respectively, $\bar{\gamma}$ is the mean value of void fraction, $\dot{m}_{int}$ is the mass flow rate at the interface of node 1 and node 2, h_{int} is the specific enthalpy at the interface and is equal to h_g, T_{w1} is the tube wall temperature at node 1, and T_{r1} is the refrigerant temperature at node 1. At the two-phase/vapor interface, refrigerant enters node 2 as saturated vapor. Therefore, $h_{int}=h_g$. Also note that ρ_l, ρ_g, h_l, h_g, and T_{r1} can be expressed as functions of pressure $P(t)$ only. Therefore, the time derivatives of $\rho_l h_l$ and $\rho_g h_g$ in equation (2.8) can be expressed in terms of the time rate of change of pressure. Hence,

$$AL_1\left(\frac{d(\rho_l h_l)}{dP}(1-\bar{\gamma})+\frac{d(\rho_g h_g)}{dP}\bar{\gamma}-\beta\right)\frac{dP}{dt}+A(1-\bar{\gamma})(\rho_l h_l-\rho_g h_g)\frac{dL_1}{dt}=$$
$$\dot{m}_i h_i-\dot{m}_{int}h_g+\alpha_{i1}\pi D_i L_1(T_{w1}-T_{r1}) \tag{2.9}$$

where β is the unit conversion constant. The mass balance equation of node 1 can be obtained by integrating equation (2.4) from $z=0$ to $z=L_1$ (see appendix for the derivation).

$$AL_1\frac{d\rho_1}{dP}\frac{dP}{dt}+A(\rho_1-\rho_g)\frac{dL_1}{dt}=\dot{m}_i-\dot{m}_{int} \tag{2.10}$$

where $\rho_1=\rho_l(1-\bar{\gamma})+\rho_g\bar{\gamma}$ is the average refrigerant density in node 1. The energy equation for the tube wall of node 1 is

$$(C_P\rho A)_w\frac{dT_{w1}}{dt}=\alpha_{i1}\pi D_i(T_{r1}-T_{w1})+\alpha_o\pi D_o(T_a-T_{w1}) \tag{2.11}$$

The energy balance equation for node 2, the superheated vapor section, is given

by:

$$AL_2\left(\rho_2\frac{dh_2}{dt}-\frac{dP}{dt}\right)=$$
$$\alpha_{i2}\pi D_iL_2(T_{w2}-T_{r2})-(\dot{m}_{int}-\rho_gA\frac{dL_1}{dt})\frac{h_o-h_{int}}{2}-\dot{m}_o\frac{h_o-h_{int}}{2} \quad (2.12)$$

where h_o is the specific enthalpy at the node 2 outlet, $h_2=(h_{int}+h_o)/2$, $\rho_2=\rho(P,h_2)$, $T_{r2}=T(P,h_2)$, and L_2 is the length of node 2. The above equation can be rewritten as:

$$AL_2\left[\left(\frac{\rho_2}{2}\frac{dh_g}{dP}-\beta\right)\frac{dP}{dt}+\frac{\rho_2}{2}\frac{dh_o}{dt}\right]=$$
$$\alpha_{i2}\pi D_iL_2(T_{w2}-T_{r2})-\frac{1}{2}(\dot{m}_o+\dot{m}_{int}-\rho_oA\frac{dL_1}{dt})(h_o-h_g) \quad (2.13)$$

The mass balance equation for node 2 is:

$$AL_2\frac{d\rho_2}{dt}+A(\rho_g-\rho_2)\frac{dL_1}{dt}=\dot{m}_{int}-\dot{m}_o \quad (2.14)$$

Since $\rho_2=\rho(P,h_2)$, the above equation can be rewritten as

$$AL_2(\frac{\partial\rho_2}{\partial P}\frac{dP}{dt}+\frac{\partial\rho_2}{\partial h_o}\frac{dh_o}{dt})+A(\rho_g-\rho_2)\frac{dL_1}{dt}=\dot{m}_{int}-\dot{m}_o \quad (2.15)$$

The energy equation for the tube wall of node 2 is

$$(C_P\rho A)_w(\frac{dT_{w2}}{dt}+\frac{T_{w1}-T_{w2}}{L_2}\frac{dL_1}{dt})=\alpha_{i2}\pi D_i(T_{r2}-T_{w2})+\alpha_o\pi D_o(T_a-T_{w2}) \quad (2.16)$$

From equation (2.10) the mass flow rate at the interface, $\dot{m}_{int}$, can be expressed in terms of other variables of interest. Thus, the $\dot{m}_{int}$ term in equations (2.9), (2.13), and (2.15) can be substituted by the expression given in equation (2.10). Equations (2.9), (2.13), (2.15), (2.11) and (2.16) are five differential equations that describe the dynamics of an evaporator in terms of five state variables: the position of the interface, L_1, refrigerant pressure P, the outlet enthalpy, $h_o(t)$, the two-phase section

tube wall temperature, T_{w1}, and the mean tube wall temperature of the superheated vapor section, T_{w2}. Given a certain set of boundary conditions in $\dot{m}_i$, h_i, and $\dot{m}_o$, equations (2.9), (2.13), (2.15), (2.11), and (2.16) can be solved for $L_1(t)$, $P(t)$, $h_o(t)$, $T_{w1}(t)$ and $T_{w2}(t)$. The superheat at the outlet of an evaporator can be determined from the values of $P(t)$ and $h_o(t)$. If these boundary conditions can be regulated at any arbitrary values, we can regard them as control inputs to affect the evaporator dynamics.

Define the vector of state variables as $\boldsymbol{x} = [L_1\ P\ h_o\ T_{w1}\ T_{w2}]^T$ and the vector of control inputs as $\boldsymbol{u} = [\dot{m}_i\ h_i\ \dot{m}_o]^T$. Then equations (2.9), (2.13), (2.15), (2.11), and (2.16) can be written in a compact state space form:

$$\dot{\boldsymbol{x}} = \boldsymbol{D}^{-1}\boldsymbol{f}(\boldsymbol{x}, \boldsymbol{u}) \tag{2.17}$$

where

$$\boldsymbol{f} = \begin{bmatrix} \dot{m}_i h_i - \dot{m}_i h_g + \alpha_{i1}\pi D_i L_1(T_{w1} - T_{r1}) \\ \dot{m}_o h_g - \dot{m}_o h_o + \alpha_{i2}\pi D_i L_2(T_{w2} - T_{r2}) \\ \dot{m}_i - \dot{m}_o \\ \alpha_{i1}\pi D_i(T_{r1} - T_{w1}) + \alpha_o \pi D_o(T_a - T_{w1}) \\ \alpha_{i2}\pi D_i(T_{r2} - T_{w2}) + \alpha_o \pi D_o(T_a - T_{w2}) \end{bmatrix} \tag{2.18}$$

and

$$\boldsymbol{D} = \begin{bmatrix} d_{11} & d_{12} & 0 & 0 & 0 \\ d_{21} & d_{22} & d_{23} & 0 & 0 \\ d_{31} & d_{32} & d_{33} & 0 & 0 \\ 0 & 0 & 0 & d_{44} & 0 \\ d_{51} & 0 & 0 & 0 & d_{55} \end{bmatrix} \tag{2.19}$$

Expressions of all elements in matrix $\boldsymbol{D}$ are given in appendix B.

Note that in equation (2.17), the heat transfer coefficient between the tube wall and air, α_o, has been considered as constant. This coefficient is in fact dependent on the air flow velocity. That is, $\alpha_o = \alpha(v_a)$, where v_a is the air velocity. For an evaporator equipped with a cross-flow fan, air velocity v_a is directly related to the fan speed. If the speed of the fan can also be continually regulated, v_a can be considered as

another control input that affects the dynamic responses of evaporator state variables. The vector of control inputs can be augmented as $\boldsymbol{u}' = [\dot{m}_i \; h_i \; \dot{m}_o \; v_a]^T$.

The dynamics of a condenser can also be formulated in the same manner into a lumped-parameter model, in which case there will be 3 nodes, including the superheated vapor node, the vapor/liquid two-phase node, and the subcooled liquid node.

2.4 Model Linearization

The state space model shown in equation (2.17) relates control inputs $\dot{m}_i$, h_i, $\dot{m}_o$, and v_a to the responses of 5 state variables of an evaporator. Although this model has been reduced to a compact, lumped-parameter form, it involves a set of nonlinear differential equations. It is desired to further simplify this model into a linear form by linearizing these differential equations around a nominal solution, say $\boldsymbol{x}^s = [L_1^s \; P^s \; h_o^s \; T_{w1}^s \; T_{w2}^s]^T$ while $\boldsymbol{u}^s = [\dot{m}_i^s \; h_i^s \; \dot{m}_o^s \; v_a^s]^T$. In most cases, an evaporator is designed to operate only in the vicinity of a predetermined operating point. The dynamic deviation from this set-point takes place only in a small amount. That is,

$$\boldsymbol{x}(t) = \boldsymbol{x}^s + \delta\boldsymbol{x}(t), \quad \boldsymbol{u}(t) = \boldsymbol{u}^s + \delta\boldsymbol{u}(t) \tag{2.20}$$

where $\delta\boldsymbol{x}(t)$ and $\delta\boldsymbol{u}(t)$ are "small" quantities compared to $\boldsymbol{x}^s$ and $\boldsymbol{u}^s$. The model that describes these dynamic deviation can be obtained as:

$$\dot{\delta\boldsymbol{x}} = \boldsymbol{A}\delta\boldsymbol{x} + \boldsymbol{B}\delta\boldsymbol{u} \tag{2.21}$$

where $\boldsymbol{A}$ and $\boldsymbol{B}$ are constant matrices and can be written as

$$\boldsymbol{A} = \boldsymbol{D}^{-1}\boldsymbol{A}' \tag{2.22}$$

$$\boldsymbol{B} = \boldsymbol{D}^{-1}\boldsymbol{B}' \tag{2.23}$$

where $\boldsymbol{D}$ is given in equation (2.19), and $\boldsymbol{A}'$ as well as $\boldsymbol{B}'$ are in the following forms.

$$\boldsymbol{A}' = \begin{bmatrix} a'_{11} & a'_{12} & 0 & a'_{14} & 0 \\ a'_{21} & a'_{22} & a'_{23} & 0 & a'_{25} \\ 0 & 0 & 0 & 0 & 0 \\ 0 & a'_{42} & 0 & a'_{44} & 0 \\ 0 & a'_{52} & a'_{53} & 0 & a'_{55} \end{bmatrix} \qquad \boldsymbol{B}' = \begin{bmatrix} b'_{11} & b'_{12} & 0 & 0 \\ 0 & 0 & b'_{23} & 0 \\ 1 & 0 & -1 & 0 \\ 0 & 0 & 0 & b'_{44} \\ 0 & 0 & 0 & b'_{54} \end{bmatrix}$$

Expressions of all elements in matrices $\boldsymbol{A}'$ and $\boldsymbol{B}'$ are given in appendix B.

The linearized model shown in equation (2.21) not only can be used for analysis of the evaporator dynamics around an operating point, it is also well suited for control design to ensure the evaporator dynamics stay within this vicinity.

Compared to the spatially distributed model, this new model of two-phase heat exchangers is simpler and mathematically tractable. Unlike the single node, lumped-parameter models which treat two-phase and one-phase sections in a heat exchanger as one single lump, this new model considers the dynamics of the these sections as separate nodes, and hence it is capable of reflecting the essential distributed characteristics such as superheat response. This model is particularly useful when incorporated into the overall model of a vapor compression cycle.

Chapter 3
Dynamic Model of a Vapor Compression Cycle

3.1 Introduction

In this chapter, we presents a new lumped-parameter dynamic model of vapor compression cycles which can be used for multivariable feedback control design.

Dynamics of a vapor compression cycle is mainly comprised of dynamics of two heat exchangers, the expansion valve model and the compressor model connecting together with appropriate boundary conditions(Figure 3.1). With the lumped-parameter moving-interface evaporator model presented in the previous chapter, a condenser models, an expansion valve model, and a compressor model, a set of state equations can be derived for the whole vapor compression cycle dynamics.

For the whole vapor compression cycle dynamics, the control inputs are compressor speed, expansion valve opening, indoor fan speed and outdoor fan speed. It is clear that the compressor speed and expansion valve opening directly affect the refrigerant flow rate. The fan speeds affect the air flow rates around the condenser and the evaporator, and in turn the air flow rates influence the heat transfer coefficients between air and these subsystems. The cycle dynamics is to provide the dynamic responses of several important variables such as evaporating temperature (or pressure), condensing temperature (or pressure), superheat, and subcool etc given a set of control inputs and ambient conditions. Using the linearized dynamics, multivariable control system can be developed to regulate several important variables at arbitrary operating points against different kinds of disturbance to maintain desired COP, or provide better transient control between different optimal set-points. The original dy-

namics is expected to be utilized for the design of optimal refrigerant control during long transient processes such as start-up. Also the whole machine nonlinear dynamics can be used for transient simulation with given control inputs. The lumped-parameter model of vapor compression cycles developed here will provide one of indispensable tools for high-performance multivariable refrigerant control design which ultimately aims at improvement of system performance and energy efficiency of air conditioning systems.

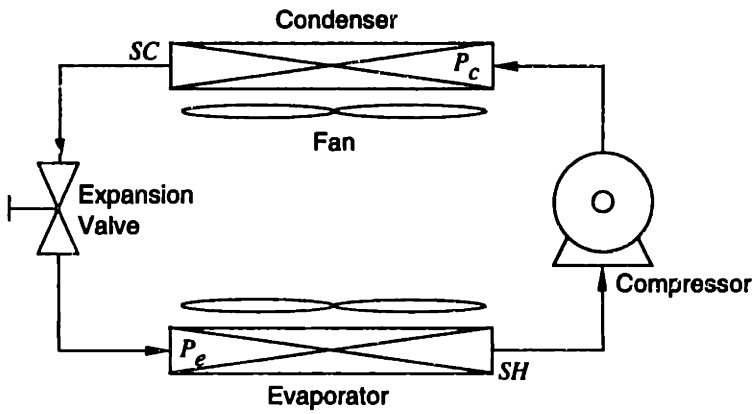

Figure 3.1: A schematic of vapor compression cycle model.

In this chapter, models for condensers, expansion valves and compressors are firstly presented. It is followed by the establish of the dynamic model for a whole vapor compression cycle. Then we discuss how to estimate all parameters involved in the dynamic model based on experimental tests as well as heat transfer and thermodynamics equations. With these estimated parameters, the new model of vapor compression cycles is simulated in a number of different cases, and is validated based on comparisons of experimental and simulation results. The model is further simplified to a lower order form to reflect the low order dynamic behavior of a vapor compression cycle.

3.2 Models of other main components

There are four main components in a vapor compression cycle, i.e., evaporator, condenser, compressor, and expansion valve. Besides these four main components, there are several additional components in an actual machine, e.g., accumulator, vapor suction and discharge lines, liquid line, four-way valve, liquid receiver, and connecting pipes etc. It is assumed that dynamics of a vapor compressor cycle around an operating point is mainly dependent on the four main components. The effects of other additional components for the cycle dynamics will be aggregately included in some parameters involved in the compressor model and expansion valve model. In this section, we discuss models for condenser, compressor and expansion valve.

3.2.1 A Lumped-Parameter Model for Condenser Dynamics

In this subsection, we derive a lumped-parameter dynamic model for a condenser. The configuration of the heat exchanger considered here is of the cross-flow type with air as the secondary fluid. By the phase of refrigerant, a condenser can be divided into three parts: a superheated vapor section, a liquid-vapor mixture section and a subcooled liquid section, as depicted in Figure 3.2. Compared with the total pressure head, the pressure drop along the condenser tube due to momentum change in refrigerant and viscous friction is negligible. Therefore, refrigerant pressure can be assumed uniform along the entire condenser tube. In the superheated vapor section, the temperature of refrigerant decreases as it travels from the inlet toward the vapor/two-phase interface. In the two-phase section, the refrigerant temperature is at its saturated value with no spatial variation. In the subcooled liquid section, the temperature of refrigerant decreases as it travels from the two-phase/liquid interface toward the outlet. For this distinction in temperature variation, we lump the con-

denser dynamics into three nodes: the superheated vapor node, the two-phase node and the subcooled liquid node.

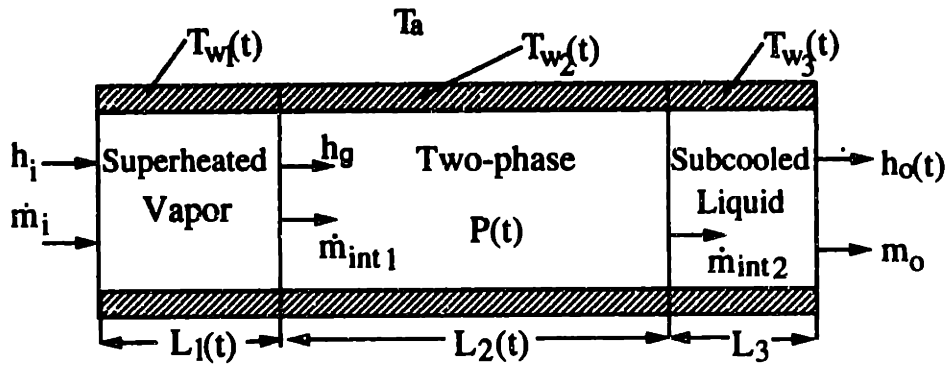

Figure 3.2: A schematic of a condenser model.

Let us consider mass flow rate at the condenser inlet $\dot{m}_i$, inflow enthalpy h_i, and mass flow rate at the outlet $\dot{m}_o$ as the boundary conditions for the governing partial differential equations of the condenser dynamics. Let $L_1(t)$ denote the length of the superheated vapor section measured from the condenser inlet, and $L_2(t)$ denote the length of the two-phase section measured from the vapor/two-phase interface. Note that $L_1(t)$ and $L_2(t)$ vary with time due to any change in boundary conditions.

The energy balance equation for node 1, the superheated vapor section, is given by:

$$AL_1\left(\rho_1\frac{dh_1}{dt}-\frac{dP}{dt}\right)=$$
$$\alpha_{i1}\pi D_i L_1(T_{w1}-T_{r1})-(\dot{m}_{int1}-\rho_g A\frac{dL_1}{dt})\frac{h_g-h_i}{2}-\dot{m}_i\frac{h_g-h_i}{2} \qquad (3.1)$$

where A is the inner area of the coil tubes, P is the condensing pressure, h_g is the saturated vapor specific enthalpy, ρ_g is saturated vapor density, h_i is the specific

enthalpy at the inlet of node 1, $h_1 = (h_i + h_g)/2$, $\rho_1 = \rho(P, h_1)$, $T_{r1} = T(P, h_1)$, $dh_1/dt = dh_g/dt$, $\dot{m}_{int1}$ is the mass flow rate at the interface of node 1 and node 2, T_{w1} is the average temperature of the tube wall of node 1, and α_{i1} is the heat transfer coefficient between the refrigerant and the tube wall at node 1.

The above equation can be rewritten as:

$$AL_1\left(\rho_1\frac{dh_g}{dP} - \beta\right)\frac{dP}{dt} =$$
$$\alpha_{i1}\pi D_i L_1(T_{w1} - T_{r1}) - \frac{1}{2}(\dot{m}_i + \dot{m}_{int1} - \rho_g A\frac{dL_1}{dt})(h_g - h_i) \tag{3.2}$$

The mass balance equation for node 1 is given by:

$$AL_1\frac{d\rho_1}{dt} + A(\rho_1 - \rho_g)\frac{dL_1}{dt} = \dot{m}_i - \dot{m}_{int1} \tag{3.3}$$

Since $\rho_1 = \rho(P, h_1)$, the above equation can be rewritten as

$$AL_1(\frac{\partial\rho_1}{\partial P} + \frac{\partial\rho_1}{\partial h_1}\frac{dh_g}{dP})\frac{dP}{dt} + A(\rho_1 - \rho_g)\frac{dL_1}{dt} = \dot{m}_i - \dot{m}_{int1} \tag{3.4}$$

The energy equation for the tube wall of node 1 is

$$(C_P\rho A)_w(\frac{dT_{w1}}{dt} + \frac{T_{w1} - T_{w2}}{L_1}\frac{dL_1}{dt}) = \alpha_{i1}\pi D_i(T_{r1} - T_{w1}) + \alpha_o\pi D_o(T_a - T_{w1}) \tag{3.5}$$

By integrating equation (2.6) from $z = L_1(t)$ to $z = L_2(t)$, we obtain the energy balance equation for node 2 (see appendix C for derivation).

$$AL_2\left(\frac{d(\rho_l h_l)}{dt}(1 - \bar{\gamma}) + \frac{d(\rho_g h_g)}{dt}\bar{\gamma} - \frac{dP}{dt}\right) + A(\rho_g h_g - \rho_l h_l)\frac{dL_1}{dt} + A\bar{\gamma}(\rho_g h_g - \rho_l h_l)\frac{dL_2}{dt} =$$
$$\dot{m}_{int1}h_g - \dot{m}_{int2}h_l + \alpha_{i2}\pi D_i L_2(T_{w2} - T_{r2}) \tag{3.6}$$

where ρ_l is saturated liquid density, h_l is saturated liquid specific enthalpy, $\bar{\gamma}$ is the mean value of void fraction of two-phase flow in node 2, $\dot{m}_{int2}$ is the mass flow rate at the interface of node 2 and node 3, T_{w2} is the tube wall temperature at node 2, and T_{r2} is the refrigerant temperature at node 2. Note that ρ_l, ρ_g, h_l, h_g, and T_{r2} can be

expressed as functions of pressure $P(t)$ only. Therefore, the time derivatives of $\rho_l h_l$ and $\rho_g h_g$ in the above equation can be expressed in terms of the time rate of change of pressure. Hence,

$$AL_2\left(\frac{d(\rho_l h_l)}{dP}(1-\bar{\gamma})+\frac{d(\rho_g h_g)}{dP}\bar{\gamma}-\beta\right)\frac{dP}{dt}+A(\rho_g h_g-\rho_l h_l)\frac{dL_1}{dt}+A\bar{\gamma}(\rho_g h_g-\rho_l h_l)\frac{dL_2}{dt}=$$
$$\dot{m}_{int1}h_g-\dot{m}_{int2}h_l+\alpha_{i2}\pi D_i L_2(T_{w2}-T_{r2}) \tag{3.7}$$

where β is the unit conversion constant. The mass balance equation of node 2 can be obtained by integrating equation (2.4) from $z = L_1$ to $z = L_2$ (see appendix C for the derivation).

$$AL_2\frac{d\rho_2}{dP}\frac{dP}{dt}+A(\rho_g-\rho_l)\frac{dL_1}{dt}+A(\rho_2-\rho_l)\frac{dL_2}{dt}=\dot{m}_{int1}-\dot{m}_{int2} \tag{3.8}$$

where $\rho_2 = \rho_l(1-\bar{\gamma})+\rho_g\bar{\gamma}$ is the average refrigerant density in node 2. The energy equation for the tube wall of node 2 is

$$(C_P\rho A)_w\frac{dT_{w2}}{dt}=\alpha_{i2}\pi D_i(T_{r2}-T_{w2})+\alpha_o\pi D_o(T_a-T_{w2}) \tag{3.9}$$

The energy balance equation for node 3, the subcooled liquid section, is given by:

$$AL_3\left(\rho_l\frac{dh_3}{dt}-\frac{dP}{dt}\right)+A\rho_l(h_l-h_3)\frac{d(L_1+L_2)}{dt}=\dot{m}_o(h_l-h_o)+\alpha_{i3}\pi D_i L_3(T_{w3}-T_{r3}) \tag{3.10}$$

where h_o is the specific enthalpy at the condenser outlet, $h_3 = (h_l + h_o)/2$, $T_{r3} = T_{r2} + (h_3 - h_l)/C_p = T_{r2} + 0.5(h_o - h_l)/C_P$. The above equation can be rewritten as:

$$AL_3\left[\left(\frac{\rho_l}{2}\frac{dh_l}{dP}-\beta\right)\frac{dP}{dt}+\frac{\rho_l}{2}\frac{dh_o}{dt}\right]+A\rho_l\frac{h_l-h_o}{2}\left(\frac{dL_1}{dt}+\frac{dL_2}{dt}\right)=$$
$$\dot{m}_o(h_l-h_o)+\alpha_{i3}\pi D_i L_3(T_{w3}-T_{r3}) \tag{3.11}$$

The mass balance equation for node 3 is:

$$\dot{m}_{int2}=\dot{m}_o \tag{3.12}$$

The energy equation for the tube wall of node 3 is

$$(C_P\rho A)_w\left[\frac{dT_{w3}}{dt}+\frac{T_{w2}-T_{w3}}{L_3}(\frac{dL_1}{dt}+\frac{dL_2}{dt})\right]=\alpha_{i3}\pi D_i(T_{r3}-T_{w3})+\alpha_o\pi D_o(T_a-T_{w3}) \tag{3.13}$$

From equation (3.4), the mass flow rate at the interface of node 1 and node 2, $\dot{m}_{int1}$, can be expressed in terms of other variables of interest. Thus, the $\dot{m}_{int1}$ term in equations (3.2), (3.7), and (3.8) can be substituted by the expression given in equation (3.4). $\dot{m}_{int2}$ in equations (3.7) and (3.8) can be replaced by $\dot{m}_o$ according to equation (3.12). Equations (3.2), (3.5), (3.7), (3.8), (3.9), (3.11) and (3.13) are seven differential equations that describe the dynamics of a condenser in terms of seven state variables: the position of the interface of node 1 and node 2, L_1, the length of the two-phase section, L_2, refrigerant pressure P, the outlet enthalpy, $h_o(t)$, and the mean tube wall temperature of the superheated vapor section, T_{w1}, the two-phase section tube wall temperature, T_{w2}, and the mean tube wall temperature of the subcooled liquid section, T_{w3}. Given a certain set of boundary conditions in $\dot{m}_i$, h_i, and $\dot{m}_o$, equations (3.2), (3.5), (3.7), (3.8), (3.9), (3.11) and (3.13) can be solved for $L_1(t)$, $L_2(t)$, $P(t)$, $h_o(t)$, $T_{w1}(t)$, $T_{w2}(t)$ and $T_{w3}(t)$. The subcool at the outlet of a condenser can be determined from the values of $P(t)$ and $h_o(t)$. If these boundary conditions can be regulated at any arbitrary values, we can regard them as control inputs to affect the condenser dynamics.

Define the vector of state variables as $\boldsymbol{x} = [L_1\ L_2\ P\ h_o\ T_{w1}\ T_{w2}\ T_{w3}]^T$ and the vector of control inputs as $\boldsymbol{u} = [\dot{m}_i\ h_i\ \dot{m}_o]^T$. Then equations (3.2), (3.5), (3.7), (3.8), (3.9), (3.11) and (3.13) can be written in a compact state space form:

$$\dot{\boldsymbol{x}} = \boldsymbol{D}^{-1}\boldsymbol{f}(\boldsymbol{x},\boldsymbol{u}) \tag{3.14}$$

where

$$\boldsymbol{f} = \begin{bmatrix} \dot{m}_i h_i - \dot{m}_i h_g + \alpha_{i1}\pi D_i L_1 (T_{w1} - T_{r1}) \\ \dot{m}_o h_g - \dot{m}_o h_l + \alpha_{i2}\pi D_i L_2 (T_{w2} - T_{r2}) \\ \dot{m}_o h_l - \dot{m}_o h_o + \alpha_{i3}\pi D_i L_3 (T_{w3} - T_{r3}) \\ \dot{m}_i - \dot{m}_o \\ \alpha_{i1}\pi D_i (T_{r1} - T_{w1}) + \alpha_o \pi D_o (T_a - T_{w1}) \\ \alpha_{i2}\pi D_i (T_{r2} - T_{w2}) + \alpha_o \pi D_o (T_a - T_{w2}) \\ \alpha_{i3}\pi D_i (T_{r3} - T_{w3}) + \alpha_o \pi D_o (T_a - T_{w3}) \end{bmatrix} \tag{3.15}$$

and

$$\boldsymbol{D} = \begin{bmatrix} d_{11} & 0 & d_{13} & 0 & 0 & 0 & 0 \\ d_{21} & d_{22} & d_{23} & 0 & 0 & 0 & 0 \\ d_{31} & d_{32} & d_{33} & d_{34} & 0 & 0 & 0 \\ d_{41} & d_{42} & d_{43} & 0 & 0 & 0 & 0 \\ d_{51} & 0 & 0 & 0 & d_{55} & 0 & 0 \\ 0 & 0 & 0 & 0 & 0 & d_{66} & 0 \\ d_{71} & d_{72} & 0 & 0 & 0 & 0 & d_{77} \end{bmatrix} \tag{3.16}$$

Expressions of all elements in matrix $\boldsymbol{D}$ are given in appendix D.

Note that in equation (3.14), the heat transfer coefficient between the tube wall and air, α_o, is dependent on the air flow velocity. That is, $\alpha_o = \alpha(v_c)$, where v_c is the air velocity. If the speed of the fan can also be continually regulated, v_c can be considered as another control input that affects the dynamic responses of condenser state variables. The vector of control inputs can be augmented as $\boldsymbol{u}' = [\dot{m}_i \; h_i \; \dot{m}_o \; v_c]^T$.

3.2.2 Models of Expansion Valves and Compressors

During normal operating conditions, the dynamics of the compressor and the expansion valve is much faster than that of the two heat exchangers. For the residential air conditioners described in the subsequent experiment section, the rise time of the compressor speed for a step change of 10 Hz is less than 4 seconds, and the rise time of the expansion valve is on the order of 100ms. In contrast, the time constant of the heat exchangers is more than 40 seconds. Therefore, the dynamics of the compressor and valve is an order-of-magnitude faster than that of the heat exchangers. In the following analysis, the compressor and the valve are treated as static components.

Expansion Valve Model

There are several different types of expansion devices available for expansion process between the condenser and the evaporator. Capillary tube, thermostatic expansion valve and electronic expansion valve are most widely used expansion devices.

A capillary tube is a long and tiny tube which can maintain the minimum pressure at the condenser at which all the flowing refrigerant can condense. For a thermostatic expansion valve, the valve opening is controlled by the counteracting pressure: the bulb pressure which measures the temperature of the refrigerant at the evaporator outlet, an opposing suction pressure which measures the pressure of the refrigerant at the evaporator outlet, and a spring pressure which provides a toggling force. Electronic expansion valves have higher performance than thermostatic expansion valve and capillary tube in several aspects like controlling refrigerant flow rate and the superheat at the evaporator exit. The opening of an electronic expansion valve is directly controlled by electronic signals determined by a certain control law. The electronic expansion valve together with inverter technology for compressor make it feasible to develop high performance multi-input multi-output(MIMO) control system for heat pumps and air conditioning systems.

Liquid refrigerant flowing through an expansion valve can simply be modeled as the following orifice equation.

$$\dot{m}_v = C_v A_v \sqrt{\rho_v \triangle P} \tag{3.17}$$

where $\dot{m}_v$ is the mass flow rate of the refrigerant through the expansion valve, C_v is the orifice coefficient, A_v is the opening area, ρ_v is the density of the refrigerant, and $\triangle P$ is the pressure drop across the orifice. Equation (3.17) shows a simple algebraic relation between the valve opening and the mass flow rate. With an electronic expansion valve, A_v is a continually adjustable variable.

Compressor Model

The compressor is the most complex component in a vapor compression refrigeration machine. It compresses the low pressure vapor refrigerant into high pressure such that the high pressure refrigerant can condense in a condenser to reject the heat to the second fluid.

It is assumed that the compressor wall is well insulated from the ambient air. Generally, the mass flow rate in air compressor is dependent on compression ratio, the compressor speed and density of the refrigerant. That is

$$\dot{m}_c = f(\frac{P_2}{P_1}, \omega, \rho) \tag{3.18}$$

where f is given by compressor performance maps, ω is compressor speed, ρ is the density of the refrigerant, and P_2 and P_1 are outlet and inlet pressures, respectively.

The relation between inlet enthalpy and outlet enthalpy is given by

$$h_{out} = \frac{h_{outs} - h_{in}}{\eta_c} + h_{in} \tag{3.19}$$

where h_{outs} is the enthalpy if the compression process is isentropic, η_c is the compressor efficient coefficient which is given by a compressor performance map.

For simplicity, we consider a simple reciprocating compressor, which is depicted in Figure 3.3. It is assumed that refrigerant flowing into the compressor undergoes a *polytropic compression*, which can be characterized by the following equation:

$$\frac{v_1}{v_2} = \left(\frac{P_2}{P_1}\right)^{1/n} \tag{3.20}$$

where v is the specific volume of refrigerant, P is pressure, and the subscripts 1 and 2 correspond to suction and discharge stages, respectively. For this simple compressor, the equation of refrigerant mass flow rate can be written as follows ([22]).

$$\dot{m}_c = \omega V_c \rho_c \left(1 + C_c - C_c(\frac{P_2}{P_1})^{1/n}\right) \tag{3.21}$$

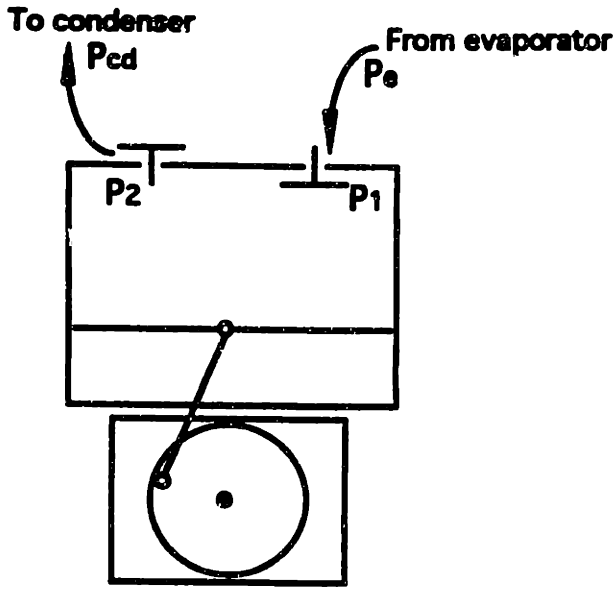

Figure 3.3: Schematic of a simple reciprocating compressor.

where $\dot{m}_c$ is the mass flow rate through the compressor, ω is the motor shaft speed, V_c is the effective displacement volume of the compressor, and n is the polytropic coefficient defined in terms of γ as:

$$n \equiv \gamma - FF(\gamma - 1) \tag{3.22}$$

where FF is a constant. It should be noted that due to the pressure drop across the intake valve and the exhaust valve, P_1 is slightly lower than the evaporator pressure, P_e, while P_2 is a bit higher than the condenser pressure, P_{cd}. Figure 3.4 gives a simplified pressure-enthalpy diagram showing the state change across the compressor.

The causality issue involved in compressor modeling is rather intricate, in addition to the complexity of the modeling task itself. One thing is certain about the compressor dynamics is that the motor shaft speed, ω can be specified at will, assuming the motor dynamics can be easily compensated. From equation (3.21), we can see that given a certain refrigerant density and $P_1 - P_2$ ratio, mass flow rate $\dot{m}_c$ is a linear function of

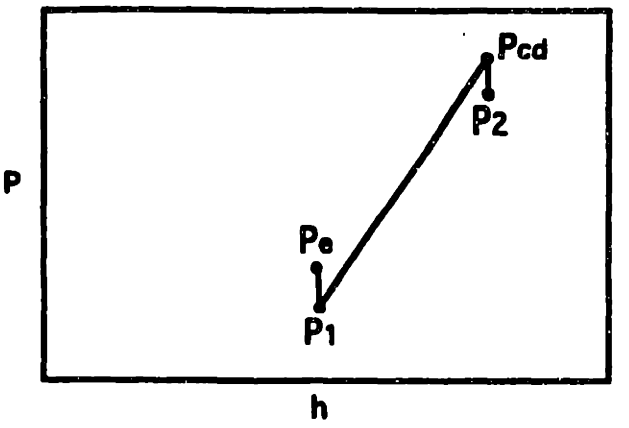

Figure 3.4: Pressure-enthalpy diagram of compressor.

ω. Note that ρ_c basically depends on the refrigerant state at the evaporator, and P_1 as well as P_2 are functions of upstream and downstream pressures. These variables are not directly related to ω. Rather, there are state variables involved in the condenser and evaporator dynamics.

3.3 Model of a whole vapor compression cycle

In addition to the compressor, valve and heat exchangers, most actual air conditioners include accumulators in the vapor compression cycle. During the normal cooling operation, such an accumulator can be regarded as a part of connecting pipes, since the accumulator is filled with vapor refrigerant and is dry throughout the normal cooling operation. Unlike a strat-up process, where the accumulator dynamics must be modeled separately, the accumulator dynamics during the normal cooling operation can be incorporated into connecting pipes.

The model of a complete vapor compression cycle can be obtained by combining the models of evaporator, condense, compressor, and expansion valve with appropriate boundary conditions. Based on the lumped-parameter evaporator and condenser models as well as the compressor model and the expansion valve model discussed

above, a lumped-parameter model can be derived for the whole vapor compression cycle dynamics.

We have already obtained the following component models.

Evaporator dynamic model

$$\dot{\boldsymbol{x}}_e = \boldsymbol{D}_e{}^{-1} \boldsymbol{f}_e(\boldsymbol{x}_e, \boldsymbol{u}_e) \tag{3.23}$$

where $\boldsymbol{x}_e$ are state variables given by

$$\boldsymbol{x}_e = [L_{e1}\ P_e\ h_{eo}\ T_{ew1}\ T_{ew2}]^T$$

and $\boldsymbol{u}_e$ are control variables for the evaporator dynamics

$$\boldsymbol{u}_e = [\dot{m}_1\ h_1\ \dot{m}_2\ v_e]^T$$

and

$$\boldsymbol{D}_e = \begin{bmatrix} d_{11} & d_{12} & 0 & 0 & 0 \\ d_{21} & d_{22} & d_{23} & 0 & 0 \\ d_{31} & d_{32} & d_{33} & 0 & 0 \\ 0 & 0 & 0 & d_{44} & 0 \\ d_{51} & 0 & 0 & 0 & d_{55} \end{bmatrix}$$

$$\boldsymbol{f}_e = \begin{bmatrix} \dot{m}_{ei}h_{ei} - \dot{m}_{ei}h_g + \alpha_{i1}\pi D_i L_{e1}(T_{ew1} - T_{er1}) \\ \dot{m}_{eo}h_g - \dot{m}_{eo}h_{eo} + \alpha_{i2}\pi D_i L_2(T_{ew2} - T_{er2}) \\ \dot{m}_{ei} - \dot{m}_{eo} \\ \alpha_{i1}\pi D_i(T_{er1} - T_{ew1}) + \alpha_o \pi D_o(T_a - T_{ew1}) \\ \alpha_{i2}\pi D_i(T_{er2} - T_{ew2}) + \alpha_o \pi D_o(T_a - T_{ew2}) \end{bmatrix}$$

Condenser dynamic model

$$\dot{\boldsymbol{x}}_c = \boldsymbol{D}_c{}^{-1} \boldsymbol{f}_c(\boldsymbol{x}_c, \boldsymbol{u}_c) \tag{3.24}$$

where

$$\boldsymbol{x}_c = [L_{c1}\ L_{c2}\ P_c\ h_{co}\ T_{cw1}\ T_{cw2}\ T_{cw3}]^T$$

and

$$\boldsymbol{u}_c = [\dot{m}_2 \; h_3 \; \dot{m}_1 \; v_c]^T$$

and

$$\boldsymbol{D}_c = \begin{bmatrix} d_{11} & 0 & d_{13} & 0 & 0 & 0 & 0 \\ d_{21} & d_{22} & d_{23} & 0 & 0 & 0 & 0 \\ d_{31} & d_{32} & d_{33} & d_{34} & 0 & 0 & 0 \\ d_{41} & d_{42} & d_{43} & 0 & 0 & 0 & 0 \\ d_{51} & 0 & 0 & 0 & d_{55} & 0 & 0 \\ 0 & 0 & 0 & 0 & 0 & d_{66} & 0 \\ d_{71} & d_{72} & 0 & 0 & 0 & 0 & d_{77} \end{bmatrix}$$

$$\boldsymbol{f}_c = \begin{bmatrix} \dot{m}_{ci}h_{ci} - \dot{m}_{ci}h_g + \alpha_{i1}\pi D_i L_{c1}(T_{cw1} - T_{cr1}) \\ \dot{m}_{co}h_g - \dot{m}_{co}h_l + \alpha_{i2}\pi D_i L_{c2}(T_{cw2} - T_{cr2}) \\ \dot{m}_{co}h_l - \dot{m}_{co}h_{co} + \alpha_{i3}\pi D_i L_{c3}(T_{cw3} - T_{cr3}) \\ \dot{m}_{ci} - \dot{m}_{co} \\ \alpha_{i1}\pi D_i(T_{cr1} - T_{cw1}) + \alpha_o \pi D_o(T_a - T_{cw1}) \\ \alpha_{i2}\pi D_i(T_{cr2} - T_{cw2}) + \alpha_o \pi D_o(T_a - T_{cw2}) \\ \alpha_{i3}\pi D_i(T_{cr3} - T_{cw3}) + \alpha_o \pi D_o(T_a - T_{cw3}) \end{bmatrix}$$

Expansion valve model

$$\dot{m}_1 = C_v A_v \sqrt{\rho_v (P_c - P_e)} \tag{3.25}$$

Compressor model

$$\dot{m}_2 = f(\frac{P_c}{P_e}, \omega) = \omega V_c \rho_c \left(1 + C_c - C_c(\frac{P_c}{P_e})^{1/n}\right) \tag{3.26}$$

$$h_3 = \frac{h_{3s} - h_2}{\eta_c} + h_2 = \frac{h_{3s}(P_e, h_2, P_c) - h_2}{\eta_c} + h_2 \tag{3.27}$$

$$h_1 = x_{c4} = h_{co} \tag{3.28}$$

In the above,

$\dot{m}_1$: the expansion valve mass flow rate (assumed to be the same as the inlet mass flow rate for the evaporator and the outlet mass flow rate for the condenser).

$\dot{m}_2$: the compressor mass flow rate (assumed to be the same as the inlet mass flow rate for the condenser and outlet mass flow rate for the evaporator).

h_1: the enthalpy at the inlet of the evaporator (assumed to be the same at the outlet of the expansion valve).

h_2: the enthalpy at the outlet of the evaporator (assumed to be the same at the inlet of the compressor).

h_3: the enthalpy at the outlet of the compressor (assumed to be the same at the inlet of the condenser).

h_4: the enthalpy at the outlet of the condenser (assumed to be the same at the inlet of the expansion valve, therefore h_4=h_1).

(the accumulator and pressure drops in the liquid line and the gas line can be compensated):

There are four control inputs, i.e. the compressor speed, two fan speeds and the expansion valve opening. Let's denote

$$u_1 = w \quad u_2 = A_v \quad u_3 = v_e \quad u_4 = v_c$$

Therefore,

$$\begin{aligned}
\dot{\boldsymbol{x}}_e &= \boldsymbol{g}_e(\boldsymbol{x}_e, \dot{m}_1, h_1, \dot{m}_2, u_3) \\
\dot{\boldsymbol{x}}_c &= \boldsymbol{g}_c(\boldsymbol{x}_c, \dot{m}_2, h_3, \dot{m}_1, u_4) \\
\dot{m}_1 &= C_v u_2 \sqrt{\rho_v (P_c - P_e)} \\
\dot{m}_2 &= f(\frac{P_c}{P_e}, u_1, \rho) \\
h_3 &= \frac{h_{3s}(P_e, h_2, P_c) - h_2}{\eta_c} + h_2 \qquad h_1 = x_{c4}
\end{aligned} \tag{3.29}$$

Based on the above equations, the dynamic model of a vapor compression cycle can be derived.

$$\dot{\boldsymbol{x}} = \boldsymbol{g}(\boldsymbol{x}, u_1, u_2, u_3, u_4) \tag{3.30}$$

where

$$\boldsymbol{x} = \{\boldsymbol{x}_e^T \quad \boldsymbol{x}_c^T\}^T$$

This nonlinear dynamic model of vapor compression cycle can be used for simulating transient responses being given any control inputs and changing ambient conditions. We are concerned with the system transient in the vicinity of a certain operating point. For this purpose, the above nonlinear matrix equation can be greatly simplified by linearizing it around a stable operating point. Linearization of this nonlinear dynamic model is discussed in details in the following section.

3.4 Model Linearization

In order to investigate the dynamic behavior of a vapor compression cycle in the vicinity of an operating point, we study the linearized model of the vapor compression cycle dynamics described by Equation (3.30).

The state space model shown in equation (3.30) relates control inputs u_1, u_2, u_3, and u_4 to the responses of all state variables of a vapor compression cycle. Although this model has been reduced to a compact, lumped-parameter form, it involves a set of nonlinear differential equations. It is desired to further simplify this model into a linear form by linearizing these differential equations around a nominal solution, say $\boldsymbol{x}^s = [(\boldsymbol{x}_e^T)^s \quad (\boldsymbol{x}_c^T)^s]^T$ while $\boldsymbol{u}^s = [u_1^s \; u_2^s \; u_3^s \; u_4^s]^T$. In most cases, a vapor compression cycle is designed to operate only in the vicinity of a predetermined operating point when the ambient conditions remain invariant. The dynamic deviation from this set-point takes place only in a small amount. That is,

$$\boldsymbol{x}(t) = \boldsymbol{x}^s + \delta\boldsymbol{x}(t), \quad \boldsymbol{u}(t) = \boldsymbol{u}^s + \delta\boldsymbol{u}(t) \tag{3.31}$$

where $\delta\boldsymbol{x}(t)$ and $\delta\boldsymbol{u}(t)$ are "small" quantities compared to $\boldsymbol{x}^s$ and $\boldsymbol{u}^s$. The model that describes these dynamic deviation can be obtained as:

$$\dot{\delta\boldsymbol{x}} = \boldsymbol{A}\delta\boldsymbol{x} + \boldsymbol{B}\delta\boldsymbol{u} \tag{3.32}$$

The matrices A and B are derived as follows.

For a linearized evaporator dynamics, we have

$$\dot{\delta\boldsymbol{x}}_e = \boldsymbol{A}_e\delta\boldsymbol{x}_e + \boldsymbol{B}_e\delta\boldsymbol{u}_e \tag{3.33}$$

where $\boldsymbol{A}_e$ and $\boldsymbol{B}_e$ are constant matrices and can be written as

$$\boldsymbol{A}_e = \boldsymbol{D}_e^{-1}\boldsymbol{A}'_e \tag{3.34}$$

$$\boldsymbol{B}_e = \boldsymbol{D}_e^{-1}\boldsymbol{B}'_e \tag{3.35}$$

where $\boldsymbol{D}_e$ is given in equation (3.3), and $\boldsymbol{A}'_e$ as well as $\boldsymbol{B}'_e$ are in the following forms.

$$\boldsymbol{A}'_e = \begin{bmatrix} a'_{11} & a'_{12} & 0 & a'_{14} & 0 \\ a'_{21} & a'_{22} & a'_{23} & 0 & a'_{25} \\ 0 & 0 & 0 & 0 & 0 \\ 0 & a'_{42} & 0 & a'_{44} & 0 \\ 0 & a'_{52} & a'_{53} & 0 & a'_{55} \end{bmatrix}_e \qquad \boldsymbol{B}'_e = \begin{bmatrix} b'_{11} & b'_{12} & 0 & 0 \\ 0 & 0 & b'_{23} & 0 \\ 1 & 0 & -1 & 0 \\ 0 & 0 & 0 & b'_{44} \\ 0 & 0 & 0 & b'_{54} \end{bmatrix}_e$$

Expressions of all elements in matrices $\boldsymbol{A}'_e$ and $\boldsymbol{B}'_e$ are given in appendix B.

For a linearized condenser dynamics, we have

$$\dot{\delta\boldsymbol{x}}_c = \boldsymbol{A}_c\delta\boldsymbol{x}_c + \boldsymbol{B}_c\delta\boldsymbol{u}_c \tag{3.36}$$

where $\boldsymbol{A}_c$ and $\boldsymbol{B}_c$ are constant matrices and can be written as

$$\boldsymbol{A}_c = \boldsymbol{D}_c^{-1}\boldsymbol{A}'_c \tag{3.37}$$

$$\boldsymbol{B}_c = \boldsymbol{D}_c^{-1}\boldsymbol{B}'_c \tag{3.38}$$

where $\boldsymbol{D}_c$ is given in equation (3.3), and $\boldsymbol{A}'_c$ as well as $\boldsymbol{B}'_c$ are in the following forms.

$$\boldsymbol{A}'_c = \begin{bmatrix} a'_{11} & 0 & a'_{13} & 0 & a'_{15} & 0 & 0 \\ 0 & a'_{22} & a'_{23} & 0 & 0 & a'_{26} & 0 \\ a'_{31} & a'_{32} & a'_{33} & a'_{34} & 0 & 0 & a'_{37} \\ 0 & 0 & 0 & 0 & 0 & 0 & 0 \\ 0 & 0 & a'_{53} & 0 & a'_{55} & 0 & 0 \\ 0 & 0 & a'_{63} & 0 & 0 & a'_{66} & 0 \\ 0 & 0 & a'_{73} & a'_{74} & 0 & 0 & a'_{77} \end{bmatrix}_c \quad \boldsymbol{B}'_c = \begin{bmatrix} b'_{11} & b'_{12} & 0 & 0 \\ 0 & 0 & b'_{23} & 0 \\ 0 & 0 & b'_{33} & 0 \\ 1 & 0 & -1 & 0 \\ 0 & 0 & 0 & b'_{54} \\ 0 & 0 & 0 & b'_{64} \\ 0 & 0 & 0 & b'_{74} \end{bmatrix}_c$$

Expressions of all elements in matrices $\boldsymbol{A}'_c$ and $\boldsymbol{B}'_c$ are given in appendix D.

According to the expansion valve model, the linearized model is

$$\delta\dot{m}_1 = \delta(C_v A_v \sqrt{\rho_v(P_c - P_e)}) = k'_{11}\delta x_{e2} + k'_{12}\delta x_{c3} + k'_{13}\delta u_2 \tag{3.39}$$

The linearized equations for compressor model are

$$\delta\dot{m}_2 = \delta f(\frac{P_c}{P_e}, u_1) = k'_{31}\delta x_{e2} + k'_{32}\delta x_{c3} + k'_{33}\delta u_1 \tag{3.40}$$

$$\delta h_3 = \delta(\frac{h_{3s}(P_e, h_2, P_c) - h_2}{\eta_c} + h_2) = k'_{21}\delta x_{e2} + k'_{22}\delta x_{c3} + k'_{23}\delta x_{e3} \tag{3.41}$$

$$\delta h_1 = \delta x_{c4} \tag{3.42}$$

where $k'_{11}, k'_{12}, k'_{13}, k'_{21}, k'_{22}, k'_{23}, k'_{31}, k'_{32}$ and k'_{33} need to be estimated experimentally.

It follows that

$$D_e\delta\dot{\boldsymbol{x}}_e = \boldsymbol{A}'_{ee}\delta\boldsymbol{x}_e + \boldsymbol{A}'_{ec}\delta\boldsymbol{x}_c + \boldsymbol{B}'_{ee}\delta\boldsymbol{u} \tag{3.43}$$

$$D_c\delta\dot{\boldsymbol{x}}_c = \boldsymbol{A}'_{ce}\delta\boldsymbol{x}_e + \boldsymbol{A}'_{cc}\delta\boldsymbol{x}_c + \boldsymbol{B}'_{cc}\delta\boldsymbol{u} \tag{3.44}$$

where $\boldsymbol{D}_e$ is given in equation (3.3), and $\boldsymbol{A}'_{ee}$, $\boldsymbol{A}'_{ec}$ and $\boldsymbol{B}'_{ee}$ are in the following forms.

$$\boldsymbol{A}'_{ee} = \begin{bmatrix} a'_{11} & a'_{12} + b'_{11}k'_{11} & 0 & a'_{14} & 0 \\ a'_{21} & a'_{22} + b'_{23}k'_{31} & a'_{23} & 0 & a'_{25} \\ 0 & k'_{11} - k'_{31} & 0 & 0 & 0 \\ 0 & a'_{42} & 0 & a'_{44} & 0 \\ 0 & a'_{52} & a'_{53} & 0 & a'_{55} \end{bmatrix}_e \quad \boldsymbol{A}'_{ec} = \begin{bmatrix} 0 & 0 & b'_{11}k'_{12} & b'_{12} & 0 & 0 & 0 \\ 0 & 0 & b'_{23}k'_{32} & 0 & 0 & 0 & 0 \\ 0 & 0 & k'_{12} - k'_{32} & 0 & 0 & 0 & 0 \\ 0 & 0 & 0 & 0 & 0 & 0 & 0 \\ 0 & 0 & 0 & 0 & 0 & 0 & 0 \end{bmatrix}_e$$

$$\boldsymbol{B}'_{ee} = \begin{bmatrix} 0 & b'_{11}k'_{13} & 0 & 0 \\ b'_{23}k'_{33} & 0 & 0 & 0 \\ -k'_{33} & k'_{13} & 0 & 0 \\ 0 & 0 & b'_{44} & 0 \\ 0 & 0 & b'_{54} & 0 \end{bmatrix}_e$$

$\boldsymbol{D}_c$ is given in equation (3.3), and $\boldsymbol{A}'_{ec}$, $\boldsymbol{A}'_{cc}$ and $\boldsymbol{B}'_{cc}$ are in the following forms.

$$\boldsymbol{A}'_{ce} = \begin{bmatrix} 0 & b'_{11}k'_{31} + b'_{12}k'_{21} & b'_{12}k'_{12} & 0 & 0 \\ 0 & b'_{23}k'_{11} & 0 & 0 & 0 \\ 0 & b'_{33}k'_{11} & 0 & 0 & 0 \\ 0 & k'_{31} - k'_{11} & 0 & 0 & 0 \\ 0 & 0 & 0 & 0 & 0 \\ 0 & 0 & 0 & 0 & 0 \\ 0 & 0 & 0 & 0 & 0 \end{bmatrix}_c$$

$$\boldsymbol{A}'_{cc} = \begin{bmatrix} a'_{11} & 0 & a'_{13} + b'_{11}k'_{32} + b'_{12}k'_{22} & 0 & a'_{15} & 0 & 0 \\ 0 & a'_{22} & a'_{23} + b'_{23}k'_{12} & 0 & 0 & a'_{26} & 0 \\ a'_{31} & a'_{32} & a'_{33} + b'_{33}k'_{12} & a'_{34} & 0 & 0 & a'_{37} \\ 0 & 0 & k'_{32} - k'_{12} & 0 & 0 & 0 & 0 \\ 0 & 0 & a'_{53} & 0 & a'_{55} & 0 & 0 \\ 0 & 0 & a'_{63} & 0 & 0 & a'_{66} & 0 \\ 0 & 0 & a'_{73} & a'_{74} & 0 & 0 & a'_{77} \end{bmatrix}_c$$

$$\boldsymbol{B}'_{cc} = \begin{bmatrix} b'_{11}k'_{33} & 0 & 0 & 0 \\ 0 & b'_{23}k'_{13} & 0 & 0 \\ 0 & b'_{33}k'_{13} & 0 & 0 \\ k'_{33} & -k'_{33} & 0 & 0 \\ 0 & 0 & 0 & b'_{54} \\ 0 & 0 & 0 & b'_{64} \\ 0 & 0 & 0 & b'_{74} \end{bmatrix}_c$$

The compact form of the linearized dynamic model of vapor compression cycle is the following.

$$\begin{bmatrix} D_e\delta\dot{\boldsymbol{x}}_e \\ D_c\delta\dot{\boldsymbol{x}}_c \end{bmatrix} = \begin{bmatrix} \boldsymbol{A}'_{ee} & \boldsymbol{A}'_{ec} \\ \boldsymbol{A}'_{ce} & \boldsymbol{A}'_{cc} \end{bmatrix} \begin{bmatrix} \delta\boldsymbol{x}_e \\ \delta\boldsymbol{x}_c \end{bmatrix} + \begin{bmatrix} \boldsymbol{B}'_{ee} \\ \boldsymbol{B}'_{cc} \end{bmatrix} \delta\boldsymbol{u} \tag{3.45}$$

Furthermore,

$$\begin{bmatrix} \delta\dot{\boldsymbol{x}}_e \\ \delta\dot{\boldsymbol{x}}_c \end{bmatrix} = \begin{bmatrix} D_e^{-1}\boldsymbol{A}'_{ee} & D_e^{-1}\boldsymbol{A}'_{ec} \\ D_c^{-1}\boldsymbol{A}'_{ce} & D_c^{-1}\boldsymbol{A}'_{cc} \end{bmatrix} \begin{bmatrix} \delta\boldsymbol{x}_e \\ \delta\boldsymbol{x}_c \end{bmatrix} + \begin{bmatrix} D_e^{-1}\boldsymbol{B}'_{ee} \\ D_c^{-1}\boldsymbol{B}'_{cc} \end{bmatrix} \delta\boldsymbol{u} \tag{3.46}$$

$$\begin{bmatrix} \delta\dot{\boldsymbol{x}}_e \\ \delta\dot{\boldsymbol{x}}_c \end{bmatrix} = \begin{bmatrix} \boldsymbol{A}_{ee} & \boldsymbol{A}_{ec} \\ \boldsymbol{A}_{ce} & \boldsymbol{A}_{cc} \end{bmatrix} \begin{bmatrix} \delta\boldsymbol{x}_e \\ \delta\boldsymbol{x}_c \end{bmatrix} + \begin{bmatrix} \boldsymbol{B}_{ee} \\ \boldsymbol{B}_{cc} \end{bmatrix} \delta\boldsymbol{u} \tag{3.47}$$

The linearized model shown in equation (3.47) not only can be used for analysis of the vapor compression cycle dynamics around an operating point, it is also well suited for control design to ensure the vapor compression cycle dynamics stay within this vicinity. This in fact is a regulator design problem where a dynamic system is to be regulated around a steady state point. In the present case, the control objective can be defined as regulating the evaporating temperature, the superheat etc in the presence of disturbance due to change in air flow temperatures or outdoor conditions as well as in any other machine components. Advanced control techniques developed for linear systems can be utilized for this regulator design problem.

3.5 Validation of the Linearized Model

In this section, we discuss validation of the present model of vapor compression cycle by comparing simulation and experimental results.

3.5.1 Experimental Set-up

In order to validate the present dynamic model of vapor compression cycles, experimental tests were conducted in the standard climate chamber which has well controlled

indoor and outdoor environment. The experimental setup is shown in figure 3.5. The air conditioner tested is a new model (Daikin AZ285SX) of residential air conditioner equipped with variable-speed compressor, variable-flow electronic expansion valve and variable-speed indoor fan. The tested machine is of split type with cooling capacity rated at 2.8KW. A schematic diagram of the test room is shown in Figure 3.6. During the tests, the indoor and outdoor conditions remains relatively invariant.

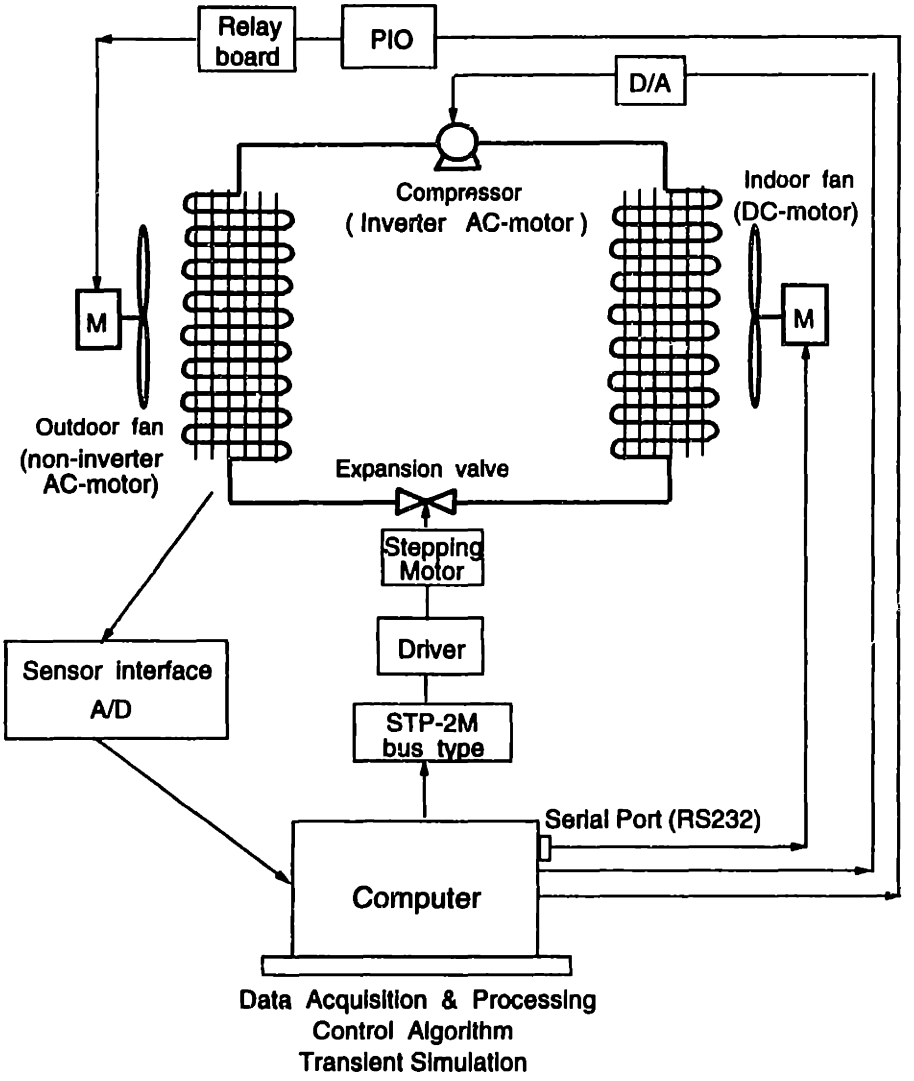

Figure 3.5: Experimental Setup

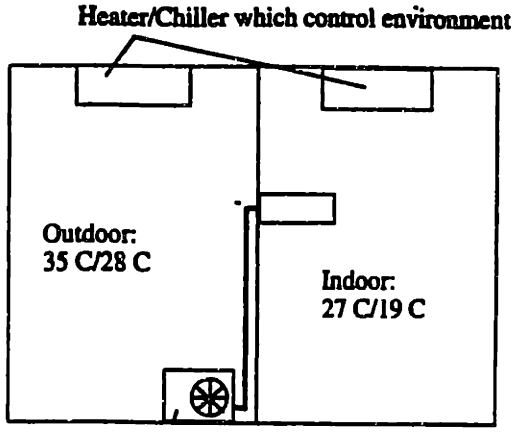

Figure 3.6: A schematic of the test room

The indoor fan motor, compressor motor and the stepping motor for the expansion valve are all controlled by the signals from a PC (Pentium/75MHz). Specifically, the indoor fan motor is controlled by RS232C serial communication commands. The compressor motor can be controlled by either way of D/A signal or RS232C serial communication commands. A stepping motor is used to control electronic expansion valve. There are 500 steps in the stepping motor. Each steps is corresponding to one 500th of full valve opening. The outdoor fan is controlled by a relay board connecting to a PIO board. Except the outdoor fan, all compressor speed, expansion valve opening and indoor fan speed are continuously adjustable.

To measure pressures, temperatures, and refrigerant mass flow rate, we installed 8 pressure sensors in different locations, 16 thermocouples to measure temperatures, and one volumetric flow meter. A semiconductor sensor built into the data acquisition board is used for reference junction compensation for thermocouples. The flow meter is of gas turbine type and is installed at the exit of indoor heat exchanger. The sensor interface consists of a A/D board for pressure signal conversion and a multiplexier board connecting a A/D board for temperature signal conversion. The volumetric flow rate is obtained by measuring voltage of a signal from the rate converter and converting the voltage value into flow rate based on calibration table. The mass

flow rate is obtained by multiplication of the density and volumetric flow rate. Heat capacity is estimated based on the enthalpy change of the refrigerant flowing through the evaporator and the mass flow rate. COP can be determined by the estimated heat capacity and the measurement of total power consumption.

3.5.2 Parameter Estimation

There are many parameters involved in the dynamic model of vapor compression cycle. Some of them can be measured directly from the machine and experimental tests, and some of them have to be estimated based on thermodynamics and heat transfer equations based on the values of the parameters and variables. In the following, we list main parameters and variable values at steady state which need to be estimated for each component, and equations to estimate these parameters.

Evaporator side

The parameters need to be estimated:

α_{i1}: average heat transfer coefficient between refrigerant at the two-phase section and the tube wall.

α_{i2}: average heat transfer coefficient between refrigerant at superheated section and the tube wall.

α_o: average heat transfer coefficient between the air and the tube wall.

$\bar{\gamma}$: mean void fraction of the two-phase section.

$(C_P \rho A)_w$: equivalent heat capacity of the tube wall.

The constants and values of variables at steady state which can be directly measured and need to be estimated :

D_i: inner diameter of the tube

D_o: outer diameter of the tube

P_e^s: the evaporating pressure at the steady state.

SH^s: superheat at the steady state.

T_{w1}^s: temperature of two-phase section tube wall at the steady state.

$\dot{m}^s$: mass flow rate at the steady state.

L_{e1}^s: length of the two-phase section at the steady state.

h_i^s: enthalpy of refrigerant at the inlet of evaporator at the steady state.

Here we mainly discuss the methods to estimate heat transfer coefficients α_{i1}, α_{i2}, and α_o, since they are very important for the model.

To estimate α_{i2}, the average heat transfer coefficient between refrigerant at superheated section and the tube wall, we use Dittus-Boelter equation for single-phase refrigerant (R-22).

$$Nu = 0.023 Re^{0.8} Pr^{0.333}$$

where

$Nu = \frac{\alpha_{i2} D_i}{k}$ is Nusselt Number.

$Pr = \frac{\mu C_P}{k}$ is Prandtl Number.

$Re = \frac{GD}{\mu}$ is Renold Number.

α_{i2} is the heat transfer coefficient need to be estimated.

$G = \dot{m}/A_i$ is refrigerant mass flux

C_P: is thermal capacity of refrigerant

k: is thermal conductivity of refrigerant

μ: absolute viscosity of refrigerant

There are two parallel pipes in the evaporator tube circuit. At a certain operating point, $\mu = 0.03 lb/ft \cdot hr$, $C_p = 0.18$, $k = 0.0058$, $\dot{m} = 88.5 lb/hr$, $A_i =$

$3.4 \times 10^{-4} ft^2$, $G = \frac{\dot{m}/2}{A_i}$. From the above equations, the estimated value of α_{i2} is $57.5 Btu/ft^2 Fhr$.

To estimate α_{i1}, the average heat transfer coefficient between refrigerant at two-phase section and the tube wall, the equation proposed by Pierre for forced convection evaporating process is used.

$$Nu = 0.0009 \cdot Re \cdot (\frac{J \triangle x i_{fg}}{L})^{0.5}$$

where

$Nu = \frac{\alpha D}{k_L}$: Nusselt Number

$Re = \frac{GD}{\mu_L}$: Renold Number

J : mechanical equivalent of heat

$\triangle x$: vapor quality change in the tube

i_{fg} : latent heat of evaporation.

k_L : thermal conductivity of liquid

μ_L : absolute viscosity of liquid

Based on the above equations, α_{i1} is estimated to be about $620 Btu/ft^2 Fhr$ for a certain operating point with $\mu_L = 0.53 lb/ft \cdot hr$, $k_L = 0.0558$, $\dot{m} = 88.5 lb/hr$, $A_i = 3.4 \times 10^{-4} ft^2$, $G = \frac{\dot{m}/2}{A_i}$.

From the above estimation, the heat transfer coefficient at the two-phase evaporating section ($\alpha_{i1} = 620 Btu/ft^2 Fhr$) is much larger than that at the superheated section ($\alpha_{i2} = 57.5 Btu/ft^2 Fhr$). If superheat value is too large, the efficiency of the evaporator becomes low since shorter section is used for evaporation. However, if the superheat is too small, there may be some liquid entering the compressor. Therefore it is important to maintain an appropriate value of superheat.

The following equation is used to estimate the length of two-phase section L_{e1}

$$\frac{\dot{m}}{2} \cdot (h_g^s - h_i^s) = \alpha_{i1} \pi D_i L_{e1} (T_{w1}^s - T_e^s)$$

where

h_i^s can be estimated based on condensing pressure and the value of subcool.

h_g^s is the enthalpy of saturated vapor which is determined by evaporating pressure.

T_{w1}^s: temperature of two-phase section tube wall at the steady state which can be directly measured.

T_e^s: evaporating temperature of two-phase refrigerant which can be directly measured.

α_o: the average heat transfer coefficient between the air and the tube wall, is estimated by empirical method as following.

$$\frac{\dot{m}}{2} \cdot (h_g^s - h_i^s) = \alpha_o \pi D_o L_{e1} (T_a - T_{w1}^s)$$

where T_a is air temperature. It should be noted that the heat transfer between evaporator tube wall and the air includes two parts. One is the sensible heat transfer between the air and the tube. The second part is the latent heat transfer which changes moist air into liquid(condensation of moist air). The estimated value of α_o is an equivalent heat transfer coefficient which represents both sensible and latent heat transfer between the air and the tube wall. The estimated value of α_o at a certain steady state is $104.5 Btu/ft^2 Fhr$.

The mean void fraction $\bar{\gamma}$ is obtained by the following equations.

$$\bar{\gamma} = \frac{\rho_l - \rho_{1b}}{\rho_l - \rho_g}$$

where

$$\rho_{1b} = \frac{1}{aL_{e1}} ln(1 + \frac{aL_{e1}}{v_0})$$

$$v_0 = v_l + x(v_g - v_l)$$

$$aL_{e1} = \frac{h_g - h_i}{h_{fg}}(v_g - v_l)$$

where v_g, v_l are specific volumes of saturated vapor and liquid. h_g, h_l are enthalpies of saturated vapor and liquid. x is the quality at the inlet of evaporator.

Condenser side

The parameters need to be estimated:

α_{i1}: average heat transfer coefficient between refrigerant at superheated section and the tube wall.

α_{i2}: average heat transfer coefficient between refrigerant at superheated section and the tube wall.

α_{i3}: average heat transfer coefficient between refrigerant at subcooled section and the tube wall.

α_o: average heat transfer coefficient between the air and the tube wall.

$\bar{\gamma}$: mean void fraction of the two-phase section.

$(C_P \rho A)_w$: equivalent heat capacity of the tube wall.

The parameters and values at steady state which can be directly measured and need to be estimated:

D_i: inner diameter of the tube

D_o: outer diameter of the tube

P_c^s: the condensing pressure at the steady state.

SC^s: subcool at the steady state.

L_{c1}^s: length of the superheated section at the steady state.

L^s_{c2}: length of the two-phase section at the steady state.

T^s_{w2}: temperature of two-phase section tube wall at the steady state.

h^s_i: enthalpy of refrigerant at the inlet of condenser at the steady state.

h^s_o: enthalpy of refrigerant at the outlet of condenser at the steady state.

To estimate the one-phase heat transfer coefficients α_{i1} and α_{i3}, we still use the Dittus-Boelter equation.

$$Nu = 0.023 Re^{0.8} Pr^{0.333}$$

To estimate the condensing heat transfer coefficient, the following equation proposed by Traviss, Baron and Rohsenow of MIT is used:

$$Nu = \frac{Re_L^{0.9} Pr_L F1^{\beta}}{F2}$$

where

$Nu = \frac{\alpha D}{k_L}$: Nusselt Number

$Re_L = \frac{G(1-x)D}{\mu_L}$: Renold Number

$Pr = \frac{\mu_L C_{P_L}}{k_L}$: Prandtl Number

$F1 = 0.15(X_{tt}^{-1} + 2.85 X_{tt}^{0.524})$

$\beta = 1 \; for \; F1 \leq 1; \beta = 1.15 \; for \; F1 > 1$

$F2 = 5Pr_L + 5ln(1 + Pr_L) + 2.5ln(0.00313 Re_L^{0.812}) \; for \; Re_L > 1125$

$X_{tt} = (\frac{1-x}{x})^{0.9} (\frac{v_L}{v_V})^{0.5} (\frac{\mu_L}{\mu_v})^{0.1}$

Based on the similar ideas for evaporator, the average heat transfer coefficient between the air and the tube wall of condenser α_o, mean void fraction $\bar{\gamma}$, L^s_{c1} and L^s_{c2} are estimated. For a certain operating point, some of steady state values are $P_e = 92.4 Psia, P_c = 200 psia, SH = 9F, SC = 2.3F$. Mass flow rate is $88.5 lb/hr$. The estimated values of the parameters are $\alpha_{i1} = 40 Btu/ft^2 Fhr, \alpha_{i2} = 710 Btu/ft^2 Fhr, \alpha_{i3} = 38 Btu/ft^2 Fhr, \alpha_o = 59 Btu/ft^2 Fhr$. There are four parallel pipes in the condenser.

Compressor side

The parameters need to be estimated:

K_{31}, K_{32}, K_{33} and K_{21}, K_{22}, K_{23}.

K_{31}, K_{32}, K_{33} are the parameters in the following equation for the change of mass flow rate through the compressor

$$\delta \dot{m}_2 = K_{31}\delta P_e + K_{32}\delta P_c + K_{33}\delta u_1$$

where u_1 is the compressor speed.

K_{21}, K_{22}, K_{23} are the parameters in the following equation for the change of refrigerant enthalpy at the exit of the compressor.

$$\delta h_3 = K_{21}\delta P_e + K_{22}\delta P_c + K_{23}\delta h_2$$

where h_2 is the refrigerant enthalpy at the compressor inlet.

To estimate K_{31}, K_{32}, K_{33}, we take the following approach.

Step 1: keep constant compressor speed and constant fan speeds, and change the expansion valve opening by step increase, and record the change of mass flow rate, the change of steady state evaporating pressure, and the change of steady state condenser pressure.

Step 2: change the indoor fan speed by step increase, and keep other control inputs constant, and record the changes of mass flow rate, evaporating pressure and condensing pressure.

Step 3: change the compressor speed by step increase, and keep other control inputs constant, and record the changes of compressor speed, mass flow rate, evaporating pressure and condenser pressure.

Based on the numbers obtained from the above three steps, the values of K_{31}, K_{32}, K_{33} can be estimated. Taking similar approach as above, K_{21}, K_{22}, K_{23} can be estimated.

Expansion valve side

The parameters need to be estimated: K_{11}, K_{12} and K_{13}.

K_{11}, K_{12} and K_{13} are the parameters in the following equation for the change of mass flow rate through the valve.

$$\delta \dot{m}_1 = K_{11}\delta P_e + K_{12}\delta P_c + K_{13}\delta u_2$$

where u_2 is the expansion valve opening. Using similar approach as above, K_{11}, K_{12}, K_{13} can be estimated.

After the values of all parameters involved in the model of vapor compressor cycle are obtained, we are ready to simulate the model with the estimated parameters.

3.5.3 Simulation of the Model and Comparisons to Experimental Results

The system considered here is a residential air conditioner of split type as described previously. Its cooling capacity is rated at 2.8 KW. We consider the cooling mode only here.

The dry bulb/wet bulb temperatures of air entering the indoor unit coil are $27^oC/19^oC$. The temperature of air entering the outdoor unit coil is 35^oC. This is the standard indoor and outdoor environment for cooling mode test. An operating point is selected where the compressor speed is $70Hz$, the expansion valve opening is 120 steps, the indoor fan speed is 1000rpm and the outdoor fan speed is 660rpm. The corresponding evaporating temperature is $Te = 8.5^oC$, the superheat is $SH = 5^oC$

The linearized dynamic model around this operating point is expressed as :

$$\dot{\delta \boldsymbol{x}} = \boldsymbol{A}\delta\boldsymbol{x} + \boldsymbol{B}\delta\boldsymbol{u} \tag{3.48}$$

$$\delta \boldsymbol{y} = \boldsymbol{C}\delta\boldsymbol{x} + \boldsymbol{D}\delta\boldsymbol{u} \tag{3.49}$$

where $\delta \boldsymbol{x}$ and $\delta \boldsymbol{u}$ are given in equation (3.31), $\delta \boldsymbol{y}$ are output variables. Under the given condition, all elements of matrices $\boldsymbol{A}$, $\boldsymbol{B}$ $\boldsymbol{C}$ and $\boldsymbol{D}$ can be obtained.

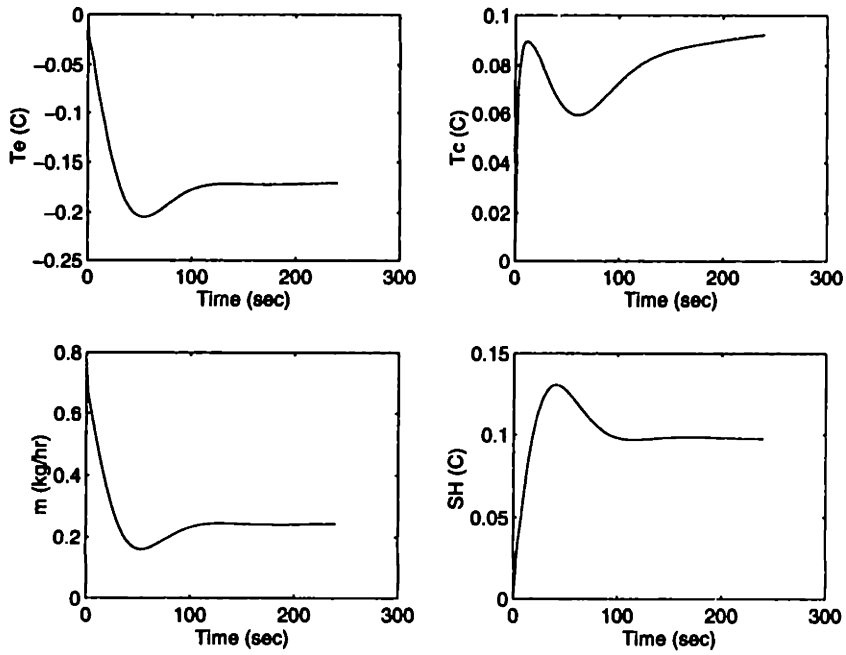

Figure 3.7: Step responses under a step change in compressor speed.

Figure 3.7 shows the dynamic responses of several variables in the model for a step increase in compressor speed. From Figure 3.7, one can see that the superheat increased with the increase of the compressor speed. Figure 3.7 also shows that the evaporating temperature decreased and condensing temperature increased when the compressor speed increased. This is indeed consistent with the intuition that a higher compressor speed will build up more compression ratio. Increase of compressor speed will increase the mass flow rate. This is shown in Figure 3.7. Step responses of the model show behavior of a low order system.

The dynamic responses of the model under a step change of the expansion valve opening are shown in Figure 3.8. A step increase of expansion valve opening implied higher refrigerant mass flow rate, which resulted in a longer two-phase section for

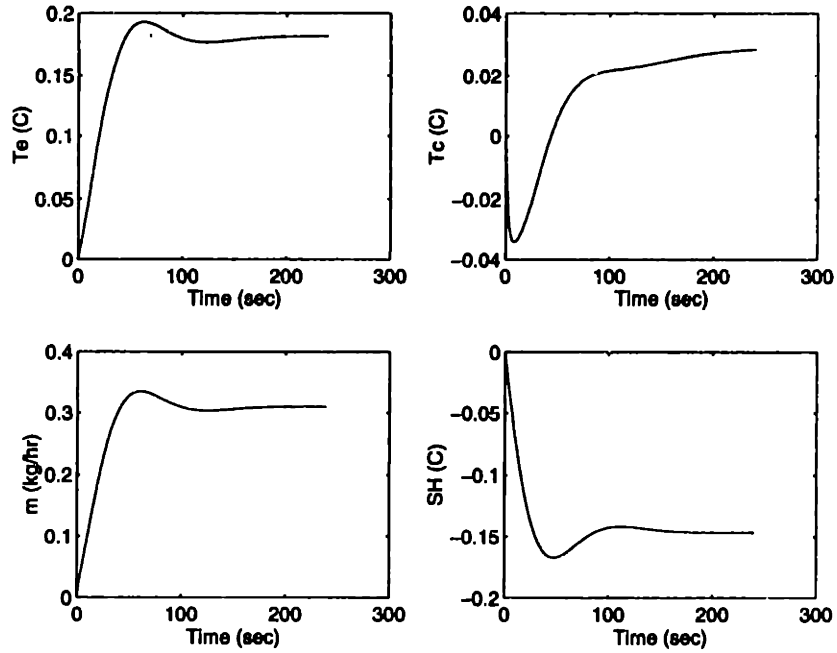

Figure 3.8: Step responses under a step change in expansion valve opening.

evaporation, and thus the superheat dropped. The increase of the opening of expansion valve gave rise to the increase of evaporating temperature The condensing temperature decreased at first when the expansion valve was open widerly, and then increased to reach a steady state.

Figure 3.9 shows the dynamic responses of several variables under a step increase of heat transfer coefficient α_o at the indoor unit side due to the change of air flow velocity which was caused by the change of the fan speed in the indoor unit. Since the heat transfer coefficient between the evaporator tube wall and the air increased, the two phase flow refrigerant evaporated more quickly. Therefore the superheat should be higher. It can be seen from Figure 3.9 that the superheat increased with an increase of the indoor fan speed. The evaporating and condensing temperatures increased due to the increase of indoor fan speed. Therefore the increase of indoor fan speed usually decrease the effort of dehumidification.

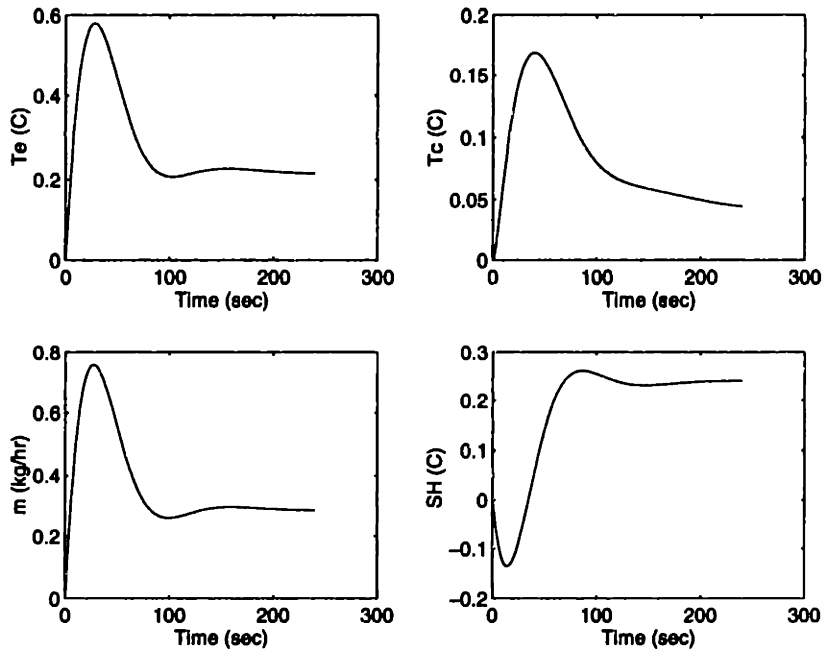

Figure 3.9: Step responses under a step increase of heat transfer coefficient α_o at the indoor unit side

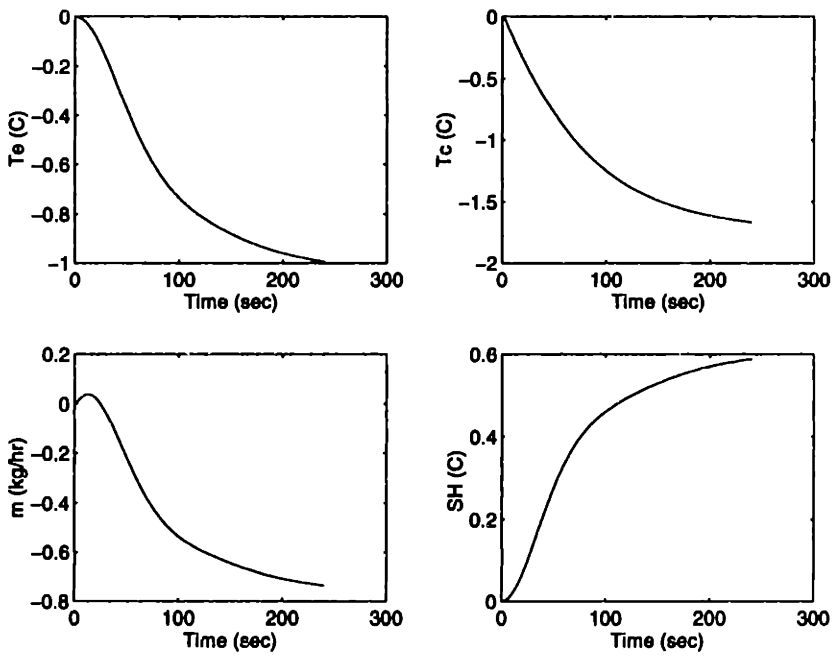

Figure 3.10: Step responses under a step change of heat transfer coefficient α_o at the outdoor unit side

Figure 3.10 shows the dynamic responses of the model under a step increase of heat transfer coefficient α_o at the outdoor unit side due to the increase of outdoor fan speed. Increase of heat transfer coefficient at the outdoor unit side makes it possible for a lower condensing temperature to reject sufficient heat to the outdoor air. It can be seen in Figure 3.10 that both the evaporating temperature and the condensing temperature decreased due to the increase of outdoor fan speed. The superheat increased with an increase of the outdoor fan speed.

Figure 3.11 shows the comparisons of simulated responses and the actual system responses measured from a experiment to a step increase in compressor speed. Figure 3.12 shows the comparisons of simulated responses and the actual system responses to a step increase in expansion valve opening.

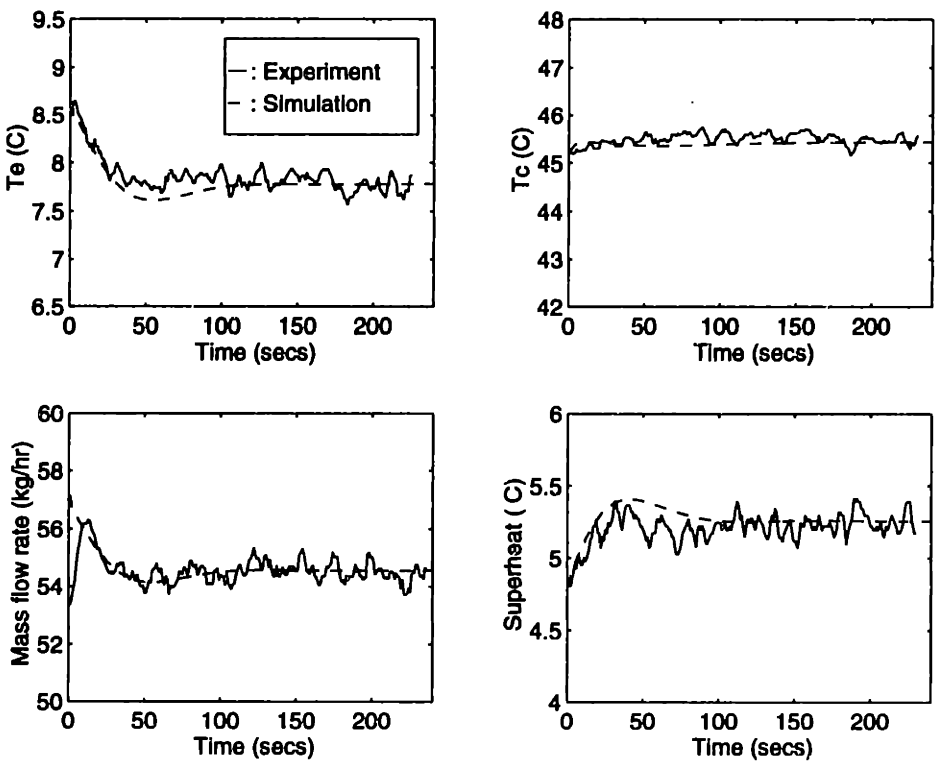

Figure 3.11: Simulated results and actual system response measured from experiments. The compressor speed is changed from 70Hz to 75Hz

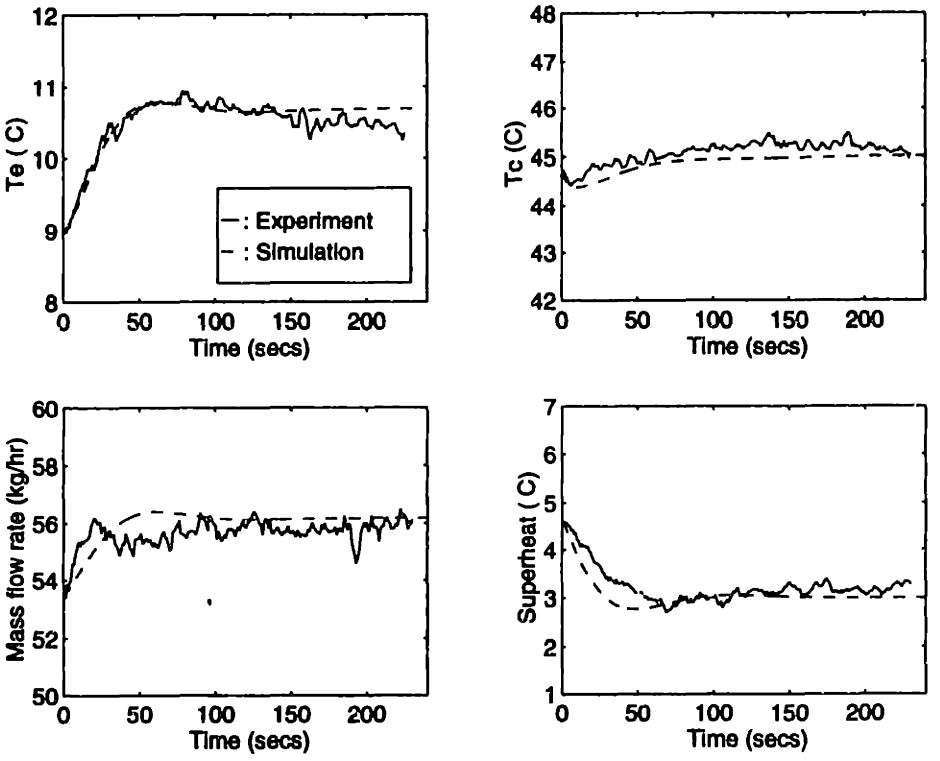

Figure 3.12: Simulated results and Actual system response measured from experiments. The expansion valve opening has 10 steps increase

From Figure 3.11 and Figure 3.12, we can see that these actual responses are consistent with the simulated ones. Both simulation and experiments show the same directions of steady state changes when a control input has a step change, and simulated responses and actual ones reflect the low order behavior of the vapor compression cycle dynamics. This implies that the analytic model captures the main characteristics of the cycle dynamics. Although the analytic model with 12 state variables has been very much simplified from the actual nonlinear, two-phase and distributive system, and there are so many parameters involved, the simulated results still match the experimental tests pretty well in terms of main dynamic characteristics and the directions of steady state changes. Therefore, the analytic model is well validated by the experiments and could be used for model-based feedback control design.

Comparisons of simulation of the model and experimental tests were also made for other operating points. Similar results were obtained.

3.6 A simplified model

Observed from the experimental tests, the actual dynamic responses of vapor compression cycles exhibit behavior of very low order systems. Therefore it is possible to further simplify the lumped-parameter dynamic model presented in the previous sections.

In both evaporator and condenser, two-phase refrigerant dominate the major portion of the heat exchangers. The thermal capacitance of these sections are much greater than that of single-phase sections. It could be seen from the eigenstructure analysis of the system matrix A that those fast eigenvalues mainly correspond to the dynamics associated with those short, single-phase sections. Hence, it is verified that the dynamics of the two heat exchangers are mainly dominated by the dynamic perturbation in the two-phase regions.

To capture only the dynamics of two-phase sections, a more simplified lumped-parameter model can be proposed as shown in Figure 3.13

Here only five independent state variables associated with the heat exchangers are defined. For the evaporator, superheat behavior is closely related to the length of the two-phase section. The dynamic behavior of P_e and SH driven by actuating inputs such as compressor speed, expansion valve opening, fan speeds can be easily derived based on this model.

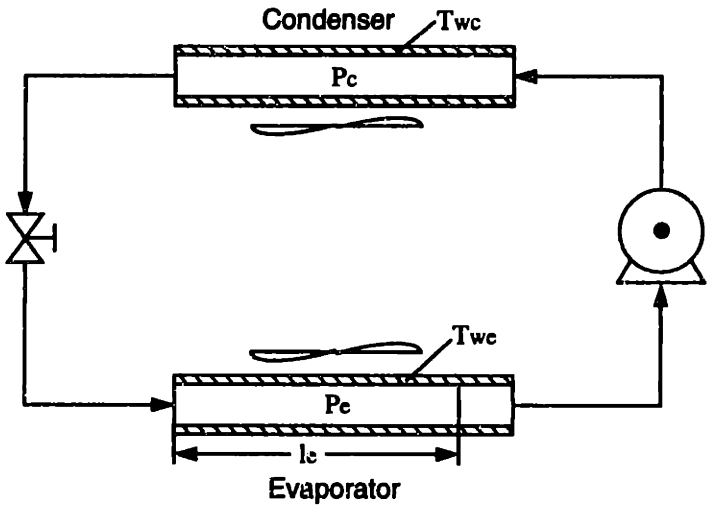

Figure 3.13: A 5-th order lumped-parameter model

Chapter 4

Multivariable Control of Vapor Compression Cycles

4.1 Introduction

Recent advances in variable-speed drive technology offer tremendous opportunities for improving system performance and energy efficiency in vapor compression systems [4]. The compressor speed can be continually adjusted so as to modulate the heat exchanger capacity to match the actual thermal load. The speeds of fans can be altered to affect the heat transfer rates across the heat exchangers. The opening of the expansion device can be varied, such as a needle valve driven by a stepper motor, so that refrigerant flow rate and pressure drop can be changed. Vapor compression systems equipped with these variable-speed and variable-position drives have already been commissioned for residential and commercial applications for several years [1]. However, to date the industry has not taken full advantage of these variable devices to gain substantial performance improvement.

One of the primary control goal in operating heat pumps and air conditioning systems is to modulate heat exchange capacity to match actual loading condition. Over the years, this has been done by running the compressor in a cyclic on-off manner. It is well known that these frequent start-up and shut-down transients result in poor energy efficiency. With today's variable-speed compressors, the cyclic on-off method has been replaced by a feedback control scheme using indoor temperature as the feedback signal. In addition to capacity modulation, superheat regulation is also essential in maximizing evaporating efficiency and in preventing liquid or excessively

heated vapor from entering the compressor. Superheat regulation has been done by merely controlling the expansion valve opening, independent of compressor speed or fan speed controls.

In principle, capacity modulation and superheat regulation have been attempted based on the conventional single-input single-output (SISO) techniques. And the performance has been limited, due to the limitation of the controller structure and the difficulty in tuning the feedback gains in the framework of SISO methodology. In addition, so far only compressor speed and expansion valve opening have been treated as active control inputs for dynamics regulation. As pointed out by [15], besides compressor speed and valve opening, the speeds of fans at the two heat exchangers are also useful inputs that should be properly controlled for improving system performance. However, the role of fan speed control has never been addressed in details in any literature.

It can be shown that there are strong cross-couplings between these various actuating inputs and performance outputs such as evaporating temperature, condensing temperature, superheat etc. By intuition, it is conceivable that a proper coordination among the valve opening, fan speeds, and compressor speed will improve superheat behavior to a greater extent in withstanding external disturbances while the system capacity being effectively modulated. In fact, advanced multi-input multi-output (MIMO) control techniques are readily available to serve this purpose.

This chapter presents multivariable feedback control design for regulating vapor compression cycles based on the dynamic model developed in the previous chapter. The control objective is defined as improving the transient behavior of the vapor compression cycle in terms of regulating desired superheat and evaporating temperature. In particular, the conventional control strategy of SISO systems is studied based on

the dynamic model and experimental tests. A model-based MIMO control design for controlling desired superheat and evaporating temperature is described. The MIMO control is digitally implemented in a residential air conditioner and compared with the SISO control experimentally.

4.2 Analysis of traditional control scheme in air conditioning systems

To date, the principle of the traditional control method for regulating the vapor compression cycle in an air conditioning system is to control indoor room temperature (or evaporating temperature T_e or cooling capacity) by the compressor speed and to regulate superheat SH by the expansion valve opening as shown in Figure 4.1. There is no feedback control for fan speeds. The indoor fan speed is set to be proportional to the compressor speed and the outdoor fan is kept to have constant speed. The two control loops are treated as two independent SISO systems, which results in a diagonal control structure (decentralized control) while the cross-couplings in the plant dynamics are completely ignored. Often a PI controller is used in the valve-superheat loop to regulate SH within a desired range, while indoor room temperature is controlled by a proportional scheme acting on the compressor speed to match the indoor thermal load during a cooling mode. For a system with cross-coupling reflected by the non-zero off diagonal terms in the transfer function matrix, such an independent SISO control invariably will result in drawbacks in its performance. It was observed long time ago that superheat controlled by thermostatic expansion valve can exhibit undesirable oscillating behavior, known as hunting phenomena [2]. This can be clearly explained by the model we proposed. In the transfer function from the expansion valve to superheat based on the model, there exists a nonminimum phase zero which stays in the right hand side of the s-plane. Figure 4.2 shows the root locus plot for the transfer

function from the valve opening a_v to the superheat SH around a certain operating point. Thermostatic expansion valve is basically a proportional controller usually with high gain. A high gain for an open loop transfer function with nonminimum phase zero will cause unstability or oscillation of the close loop system. If a small gain is used for the P-controller, the closed loop response will have steady state error, although it may be stable.

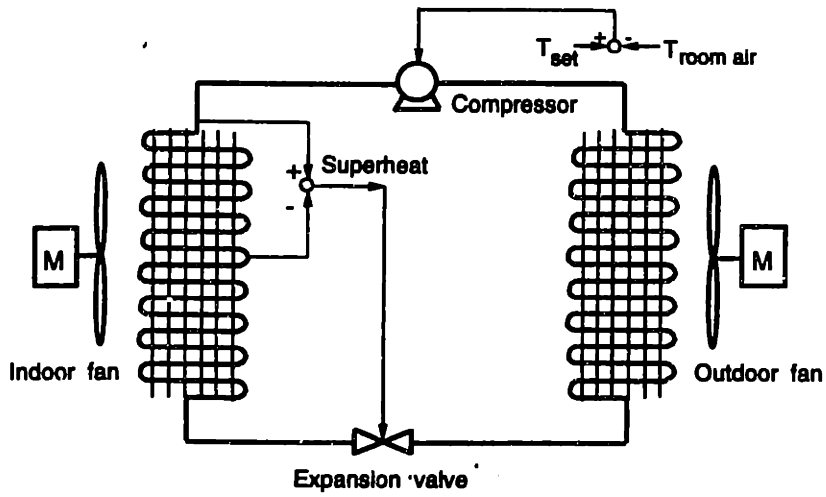

Figure 4.1: A decouple SISO control system

PID controller was proposed to regulate the superheat using a motor driven needle

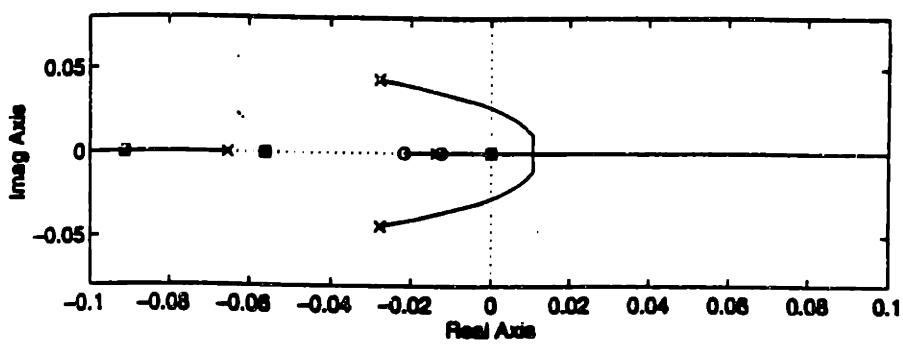

Figure 4.2: Root locus of the transfer function from a_v to SH (partially shown here)

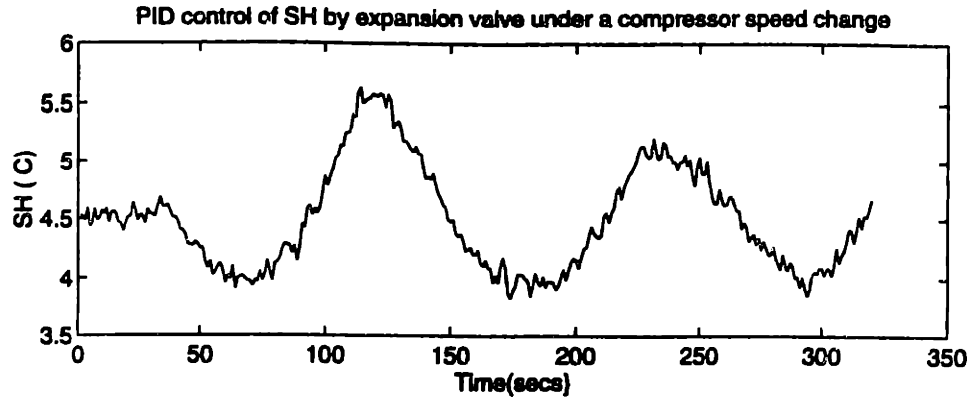

Figure 4.3: Valve-controlled SH response to a step change in compressor speed.

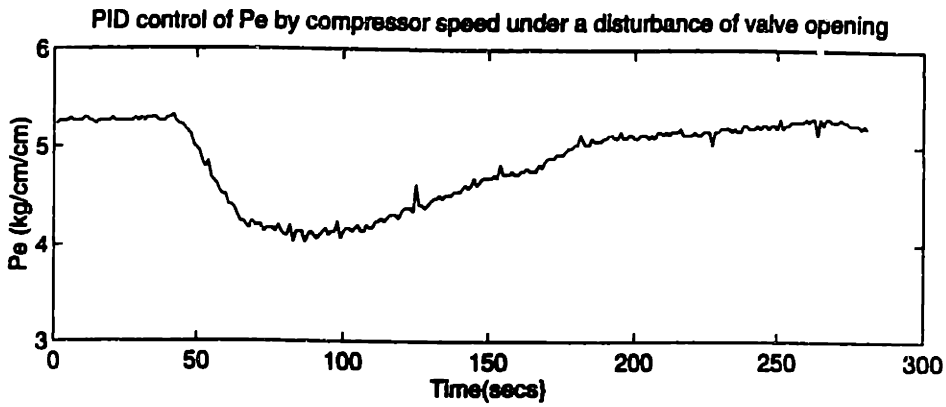

Figure 4.4: Compressor-controlled P_e response to a step change in valve opening.

expansion valve in [10] to avoid steady state error. However there is strong coupling between superheat and compressor speed. Figure 4.3 shows the response of valve-controlled SH (PI controller) to a step change in compressor speed. It can be seen that the transient process takes a long time to reach the desired steady state. There is no way to adjust PID controller parameter to get a quick response without causing oscillation or large undershoot. Figure 4.4 shows the response of compressor-controlled P_e(PI-controller) to a step change in valve opening. It can be seen that the transient process is long and has undesired undershoot. As shown in Figure 4.3 and Figure 4.4, a poor coordination between compressor speed and valve opening in the presence of strong cross-couplings can result in unfavorable interference between the two loops.

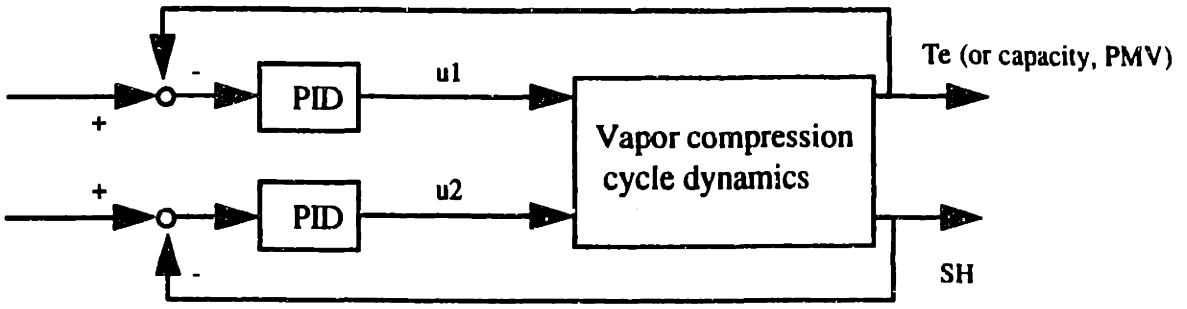

Figure 4.5: A decouple SISO control system

The conventional control system for regulating the evaporating temperature T_e and the superheat SH is illustrated in Figure 4.5. Two control loops are decoupled. Since there exist strong cross-coupling between these two control loops, the performance of the conventional SISO system is very limited.

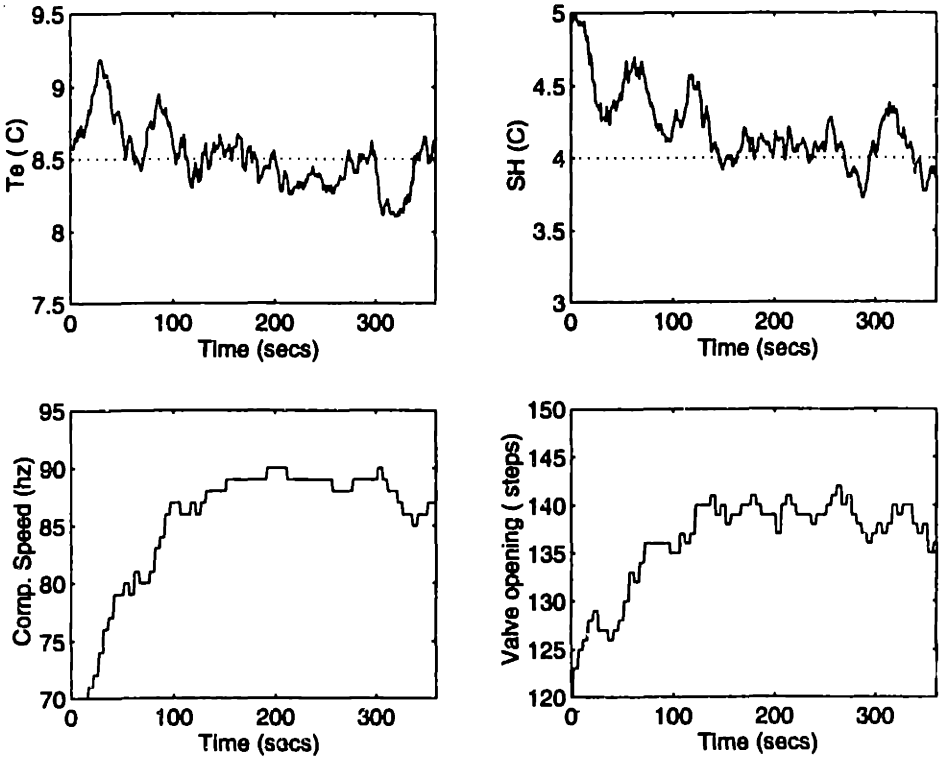

Figure 4.6: Performance of a SISO control system

Figure 4.6 shows the performance of the SISO control system if the gains are tuned based on Zigler-Nicoles optimal gain tuning method for PI controller. In Figure 4.6, the control objective is to reduce the desired superheat valve from 5°C to 4°C while evaporating temperature is kept at 8.5°C. It is observed that the control system is oscillating. To avoid unstable or oscillating performance, small gains must be used. That generally causes slow transient processes.

4.3 Model-based MIMO control of vapor compression cycles

4.3.1 A multivariable control design method: LQG with integrator

In order to better control the transient processes of vapor compression cycles, model-based multivariable control is presented. Based on the dynamic model of a vapor compression cycle developed in the previous chapter, multivariable control systems can be designed to control T_e and SH by both compressor speed and expansion valve opening. Figure 4.7 shows the schematic diagram of a MIMO control system. The main difference is that the decoupled SISO control only use one feedback signal to generate one control input. However MIMO controls use both feedback signals to generate two control inputs. When a dynamic model is used to design a MIMO control, the cross coupling between the two single SISO loops can be taken into account. That makes the MIMO control have better performance than the decoupled SISO control, since the two SISO loops are strongly coupled.

Based on the dynamic model, we designed multivariable controllers to control vapor compression cycle. The particular objective of control here is to regulate superheat and evaporating temperature by both compressor speed and expansion valve opening. The multivariable control method which is used here is Linear-Quadratic Gaussian(LQG) control with integrator because this MIMO control can optimize a cost function which

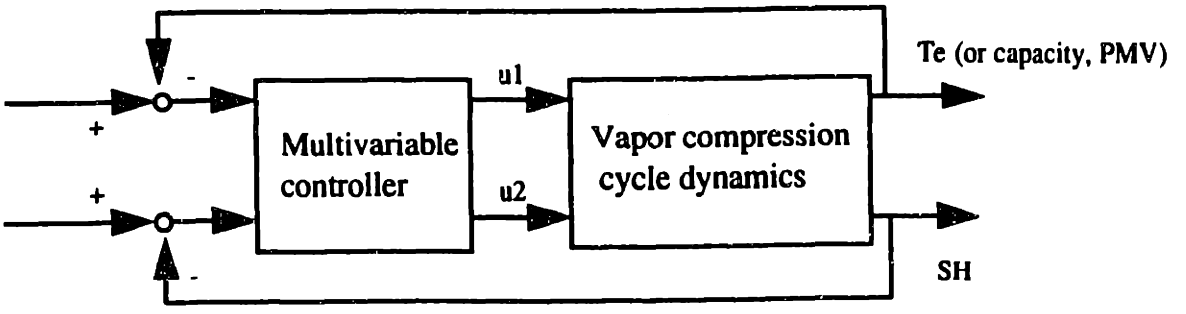

Figure 4.7: A multivariable control system

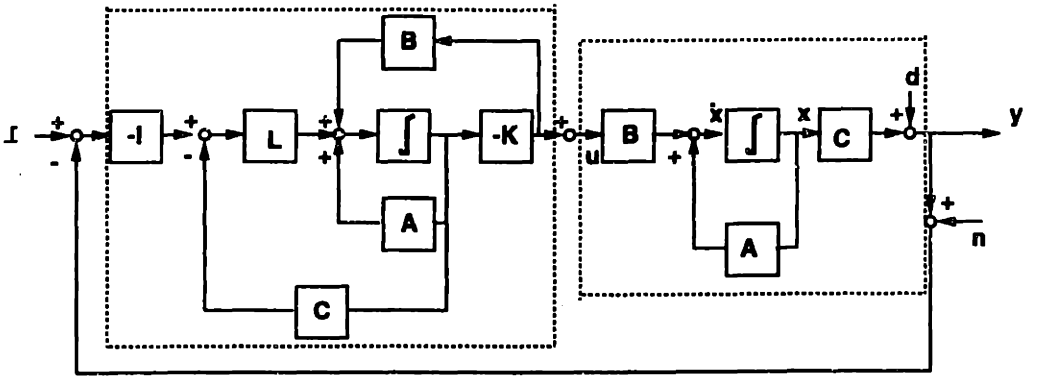

Figure 4.8: A block diagram of LQG

compromises the output errors and control efforts.

The structure of a LQG multivariable controller is shown in Figure 4.8. It is an observer-based compensator which uses Kalman filter to optimally estimate unmeasured state variables based on measurements and then use the optimal full state feedback to generate the control law. The optimal gain matrix K and Kalman filter matrix L are determined based on the system matrix A, B, C, D of the dynamic model and weighting matrices Q and R for linear quadratic regulator and weighting matrices Q and R for linear quadratic estimator.

The dynamic model of a vapor compressor cycle around an operating point is expressed in a state space form as follows.

$$\dot{\mathbf{x}} = A\mathbf{x} + B\mathbf{u} \tag{4.1}$$

$$\mathbf{y} = C\mathbf{x} + D\mathbf{u} \tag{4.2}$$

where $\mathbf{x}$ are the state variables, $\mathbf{u}$ are control inputs, and $\mathbf{y}$ are system outputs. And $D = 0$.

The optimal feedback gain matrix K is calculated such that the feedback law $\mathbf{u} = -K\mathbf{x}$ minimizes the cost function:

$$J = \int (\mathbf{y}'Q\mathbf{y} + \mathbf{u}R\mathbf{u})dt \tag{4.3}$$

subject to the constrain equation:

$$\dot{\mathbf{x}} = A\mathbf{x} + B\mathbf{u}, \quad \mathbf{y} = C\mathbf{x} + D\mathbf{u}$$

To obtain Kalman filter gain matrix L, linear quadratic estimator design is considered. For the system:

$$\dot{\mathbf{x}} = A\mathbf{x} + B\mathbf{u} + B\mathbf{w} \tag{4.4}$$

$$\mathbf{y} = C\mathbf{x} + D\mathbf{u} + \mathbf{v} \tag{4.5}$$

with process moise and measurement moise covariances:

$$E\{\mathbf{w}\} = E\{\mathbf{v}\} = 0,\ E\{\mathbf{w}\mathbf{w}'\} = Q,\ E\{\mathbf{v}\mathbf{v}'\} = R,\ E\{\mathbf{w}\mathbf{v}'\} = 0$$

The gain matrix L is obtained such that the stationary Kalman filter

$$\dot{\mathbf{x}} = A\mathbf{x} + B\mathbf{u} + L(\mathbf{y} - C\mathbf{x} - D\mathbf{u}) \tag{4.6}$$

produces an linear quadratic Gaussian optimal estimate of state variables $\mathbf{x}$ based on the measurement output $\mathbf{y}$ and the state equations.

After gain matrix K and L are obtained, the transfer function of the observer-based compensator LQG can be expressed as

$$C(s) = K(sI - A + BK + LC)^{-1}L$$

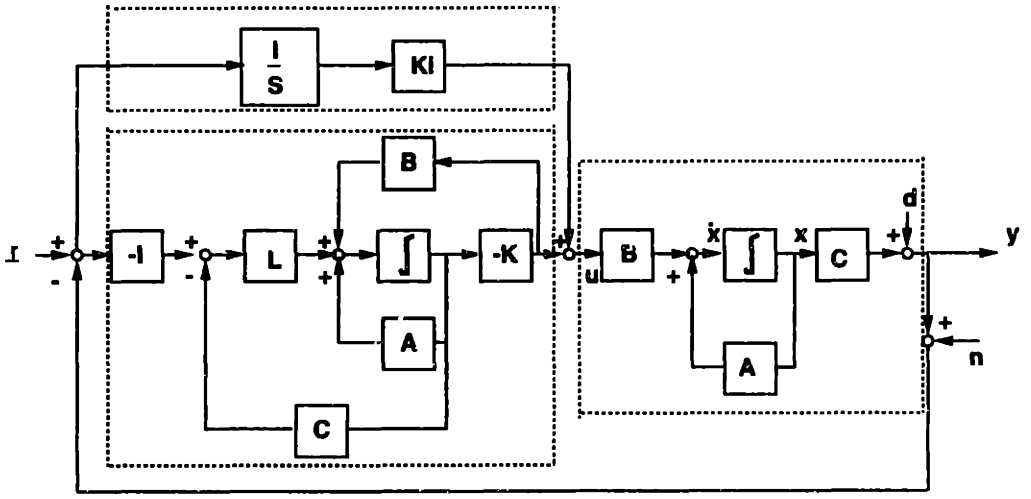

Figure 4.9: A block diagram of LQG with integrators

Generally, a LQG control will have steady state error if the plant itself has no integrator. Therefore, for vapor compressor cycles which have no integrator in the dynamics, we need to include the integrator in LQG to eliminate steady state errors, Figure 4.9 shows the block diagram of LQG with integrator. To design a LQG with integrator based on the dynamic model, we at first need to include the integrators in the model, and then augment the states to include integrator variables. All outpus, integrator variables and control inputs are included in the cost function to be optimized.

Integration of y give rise to the integrator variables z.

$$\dot{\mathbf{z}} = I\mathbf{y} \tag{4.7}$$

The augmented state is

$$\mathbf{x}_a = \begin{bmatrix} x \\ z \end{bmatrix}$$

Therefore the augmented state equations are

$$\dot{\mathbf{x}}_a = \begin{bmatrix} A & 0 \\ C & 0 \end{bmatrix} \mathbf{x}_a + \begin{bmatrix} B \\ 0 \end{bmatrix} \mathbf{u}$$

$$\mathbf{y}_a = \begin{bmatrix} C & 0 \\ I & 0 \end{bmatrix} \mathbf{x}_a$$

The optimal feedback gain matrix for the augmented system is obtaibed such that the feedback law $\mathbf{u} = -K_a\mathbf{x}_a$ minimizes the cost function:

$$J = \int (\mathbf{y}_a' Q \mathbf{y}_a + \mathbf{u} R \mathbf{u}) dt \tag{4.8}$$

subject to the constrain of the augmented system state equations.

After the optimal feedback gain matrix K_a is obtained, the control law can be expressed in the summation of two terms

$$u = -K_a\mathbf{x}_a = -[K \; K_I] \begin{bmatrix} x \\ z \end{bmatrix} = -K\mathbf{x} - K_I\mathbf{z} \tag{4.9}$$

MIMO control for a vapor compression cycle can be designed based on the above procedures.

4.3.2 Digital implementation and Experimental results

The multivariable control has been digitally implemented for the tested machine. Five second sampling time was selected based on the main time constant of the system. The control input (compressor speed and expansion valve) are therefore generated based on the multivariable control law and the feedback signals of superheat SH and evaporating temperature Te.

In the design of the LQG with integrator, the bandwidth frequency is selected to be 0.1 rad/sec. The dominant frequency of the vapor compression cycle around the given operating point is about 0.05 rad/sec. Figure 4.10 shows the singular valve of the dynamic model transfer function, the loop transfer function(with controller), the closed loop transfer function and the sensitivity transfer function. The design has about 0.1 rad/sec closed loop bandwidth, and can tolerate about $w/0.1$ model error and have guaranteed performance error of less than $w/0.04$ for frequency less than 0.01 rad/sec.

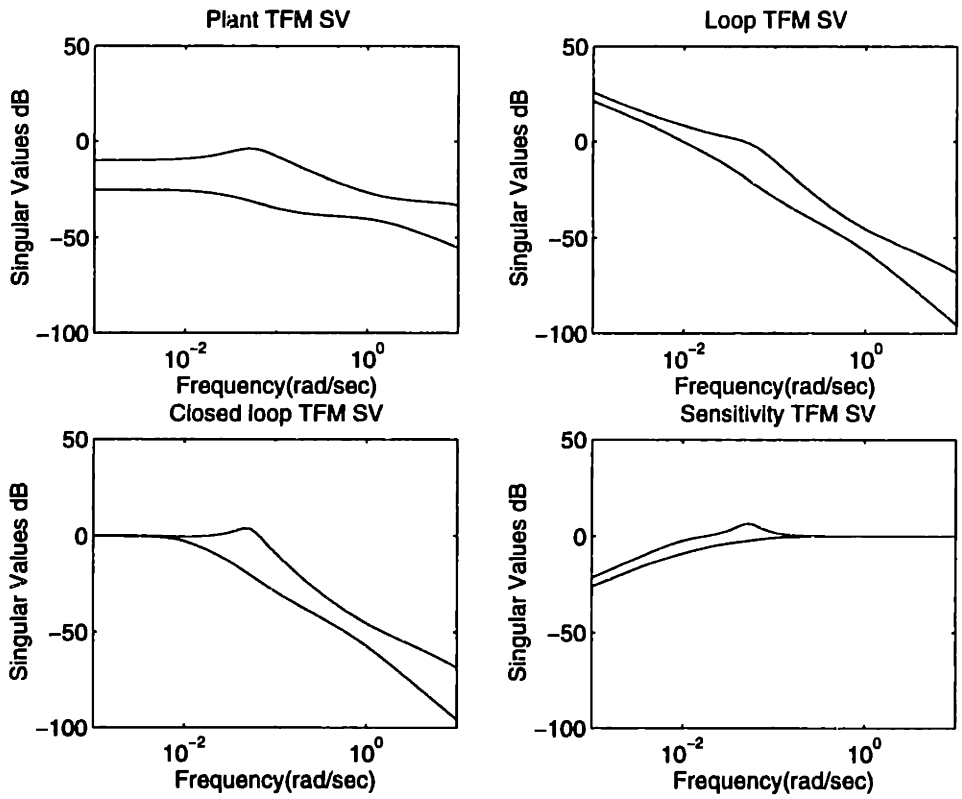

Figure 4.10: Frequency domain singular values

To compare the command following capability of the MIMO control and the SISO control, the SISO control gains are best tuned. Figure 4.11 shows the results when

the desired evaporating temperature Te is changed from 8.5°C to 7°C while the superheat value SH remains at 5°C. Figure 4.12 shows the comparisons when the desired superheat value is changed from 5°C to 4°C. It can be seen that the MIMO control has much better performance than the SISO control in command following. For the SISO control, it takes about 4 to 6 minutes to reach steady state, however the MIMO control can reach steady state in 2 to 3 minutes. By utilizing the dynamic model and the coordination of two control inputs, the transient processes controlled by the MIMO system are much faster.

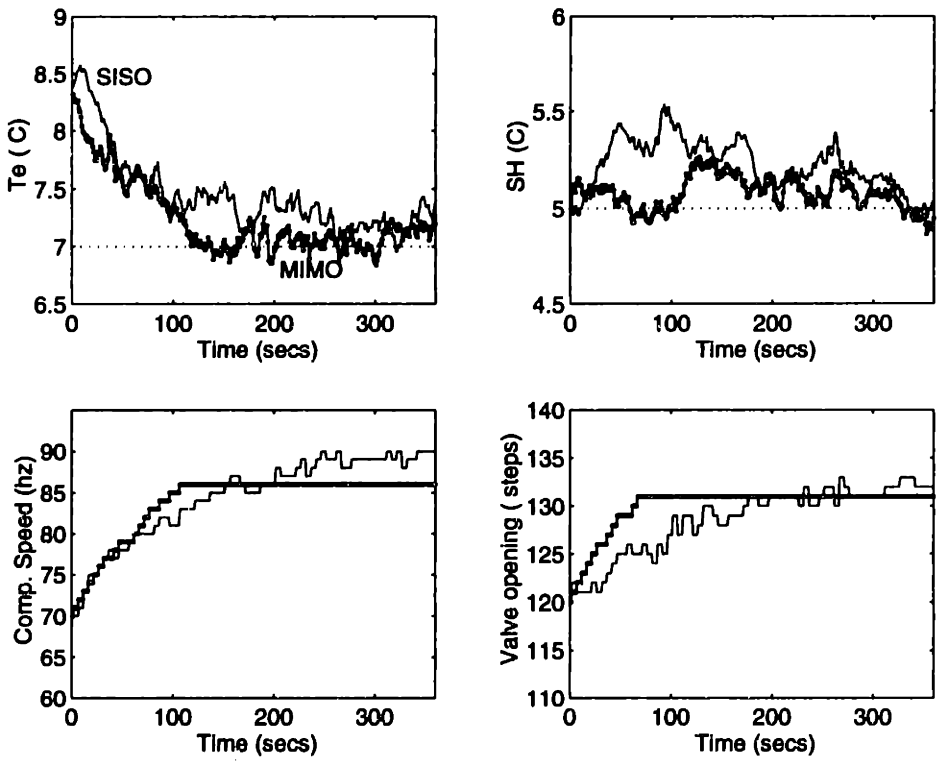

Figure 4.11: Command following: Desired Te has a step change

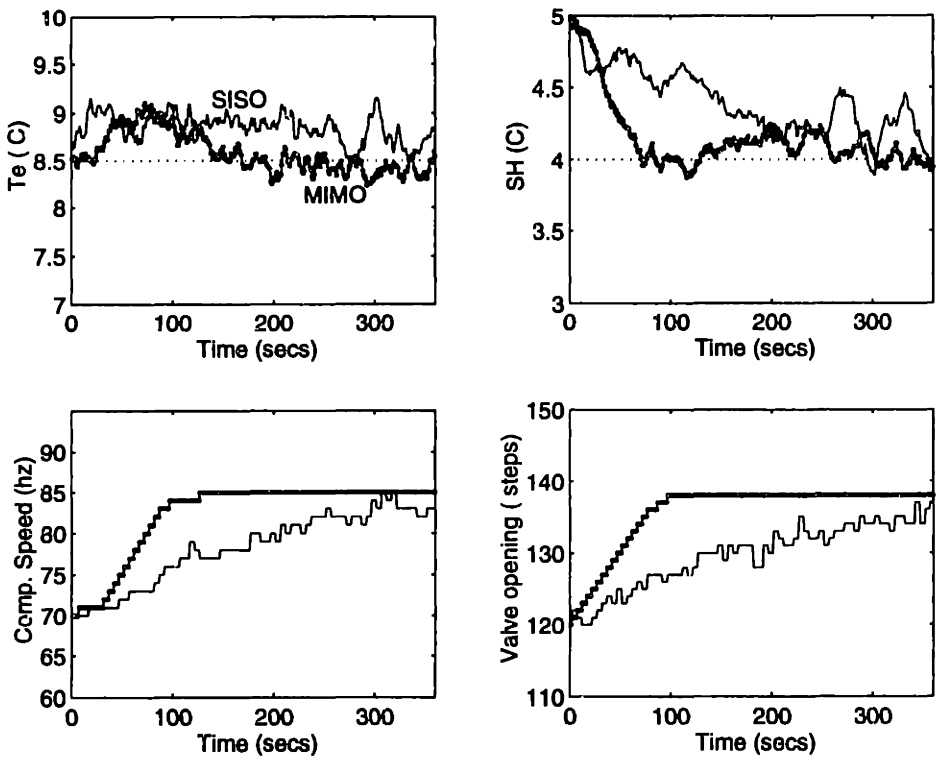

Figure 4.12: Command following: Desired superheat has a step change

The disturbance rejection capability was tested both for the MIMO control and the SISO control. In the disturbance rejection tests, the desired superheat and evaporating temperature need to remain the same after the indoor fan speed is changed from 1000rpm to 1200 rpm. Figure 4.13 shows the comparison results. It can be observed that the MIMO control has much better disturbance rejection capability that the SISO control as predicted in the previous section.

It is important to investigate the effects of high control gains and model errors on MIMO control stability and performance. Since there must exist a certain level of uncertainty in the dynamic model used for control design, too high control gains will enlarge the effect of model errors and actuators dynamics on the control stability. It

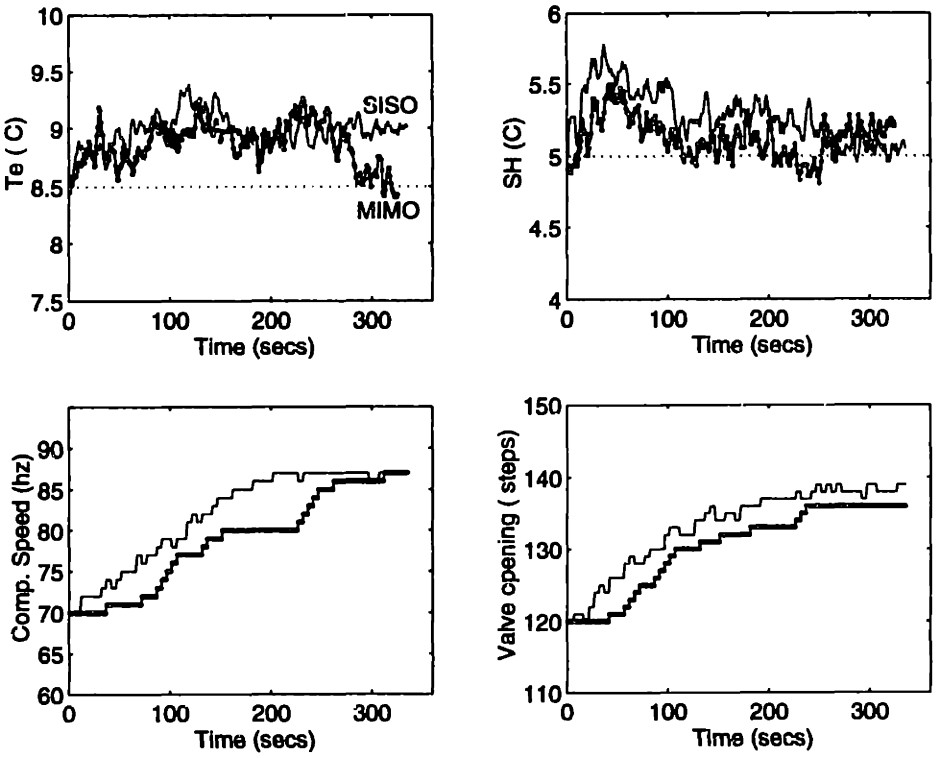

Figure 4.13: Disturbance rejection: indoor fan speed changed from 1000rpm to 1200rpm

turns out that the closed loop maximum singular valves could go bevond the robustness bound. Figure 4.14 shows that if too high gains were used in MIMO control design, it caused unstability of the closed loop system. Therefore, we need to select appropriate control gains for MIMO control. The effects of model errors on the MIMO control stability are also tested. It turned out that the closed loop system is still robustly stable even if the evaporating heat transfer coefficient or the mean void fraction has 50% change.

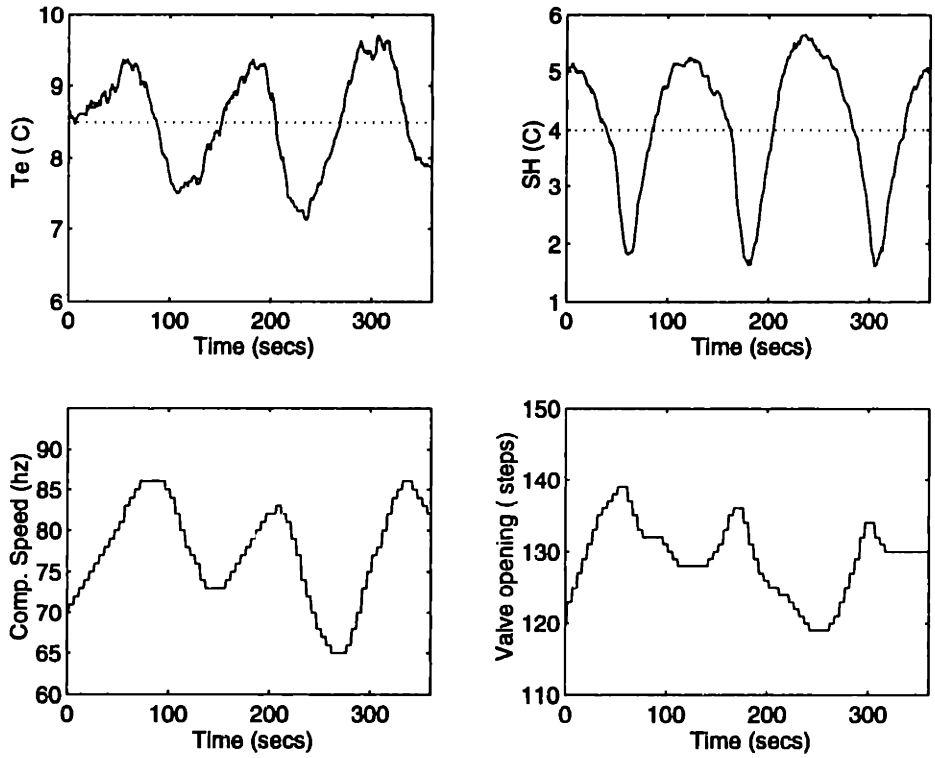

Figure 4.14: Effect of high control gain

4.3.3 Control of vapor compression cycle over a wide range using gain scheduling scheme

It is desirable to control vapor compression cycle over a wide range based on MIMO controls. Since system nonlinearities become evident over a wide range of operating conditions, it is important to adapt the control law to different operating range using gain scheduling technique. A schematic diagram of gain scheduling is shown in Figure 4.15. Figure 4.16 shows the control results over a wide range. The control goal in Figure 4.16 is that the desired evaporating temperature needs to be changed from 7°C to 10°C while the superheat is kept to be 4.5°C. From Figure 4.16, one can see that the

compressor speed is changed about 40 Hz which is almost 50% operating range. We used two MIMO control laws for two operating points and successfully controlled the desired evaporating temperature and superheat. It can be seen that the MIMO control is much faster than the SISO control. In this situation, since the transient process controlled by the MIMO system is much quicker than that of the SISO control, the COP is significantly different as shown in Figure 4.17. The desired capacity can be reached much faster by use of MIMO control.

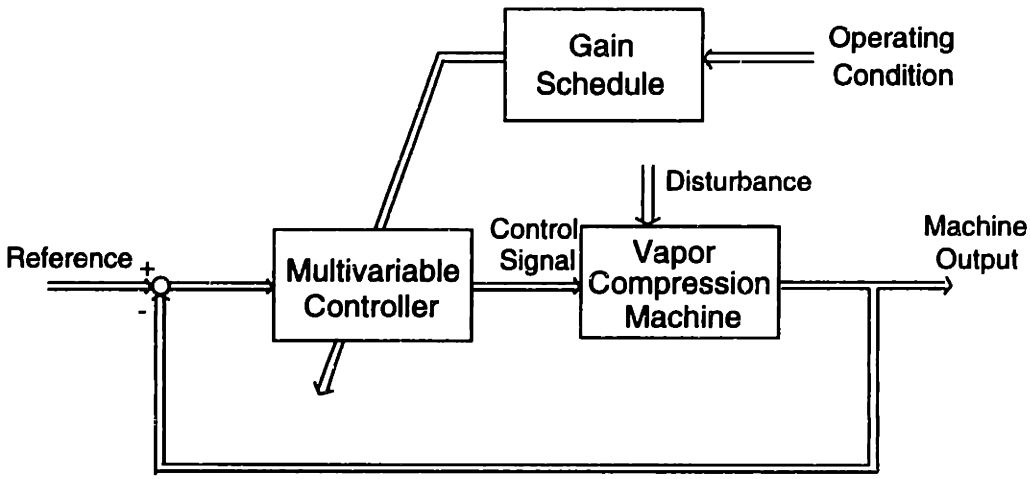

Figure 4.15: A schematic of gain schedule

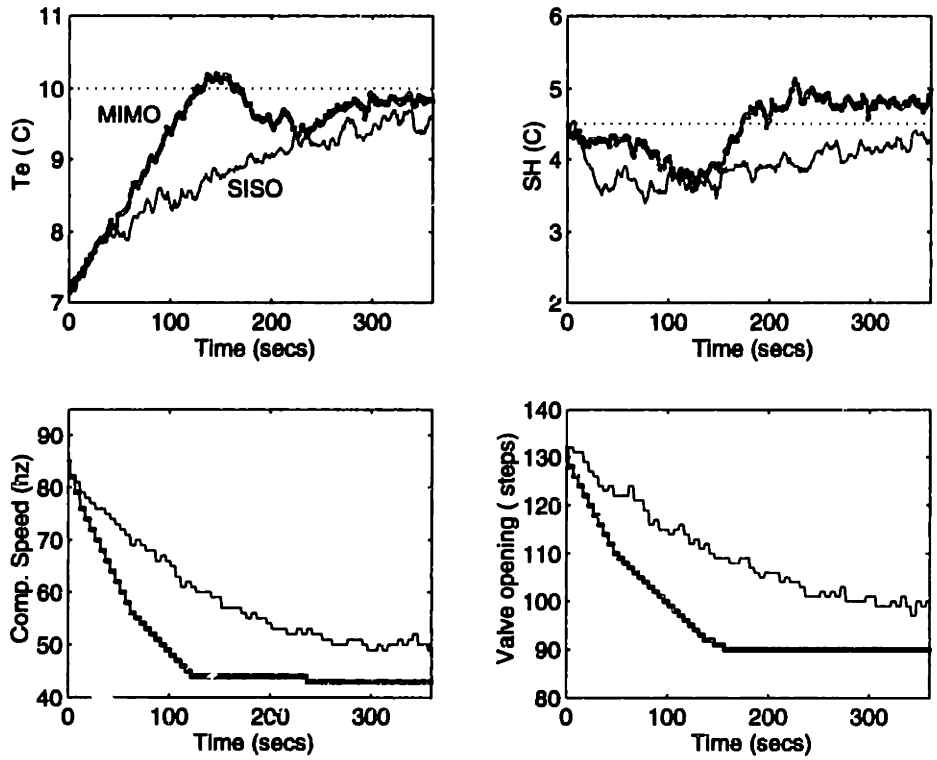

Figure 4.16: Control of vapor compression cycle in a wide range

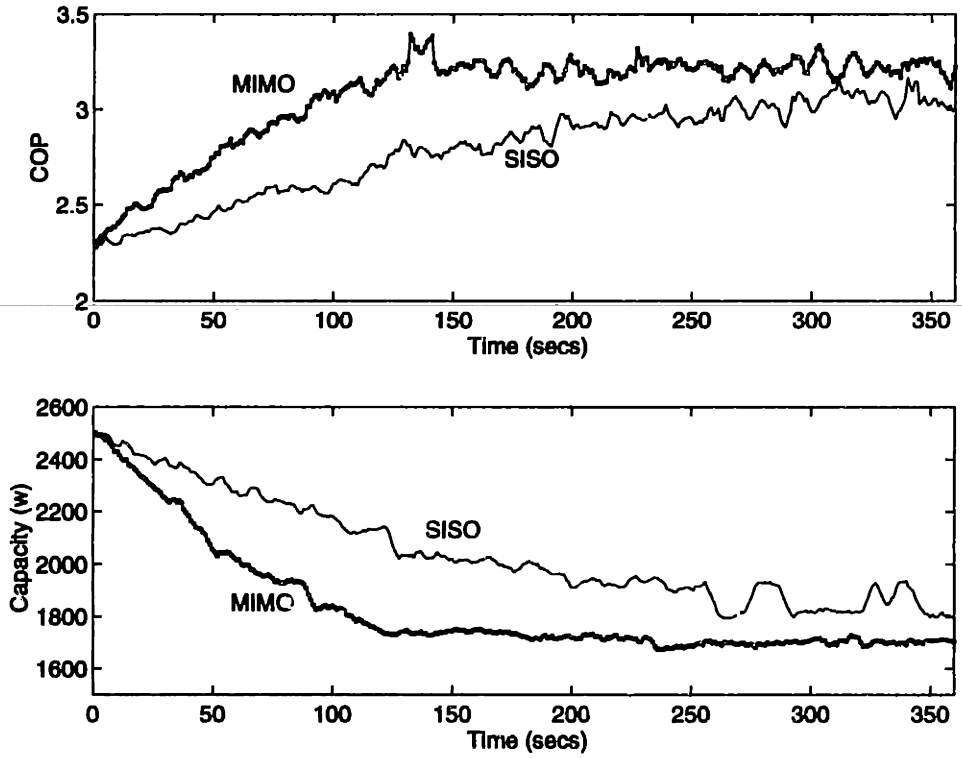

Figure 4.17: COP and cooling capacity of the MIMO control and the SISO control

Chapter 5
Conclusions

5.1 Thesis Summary

The main results and contributions of this thesis are summarized as follows:

A moving-interface model of two-phase heat exchangers

A two-node moving-interface lumped-parameter model has been presented for describing the dynamics of two-phase flow heat exchanger. Compared to the spatially distributed model, this new model is simpler and mathematically tractable for control design. Unlike the single node, lumped-parameter models which treat two-phase and one-phase sections in a heat exchanger as one single lump, this new model considers the dynamics of these sections as separate nodes, and hence it is capable of reflecting the essential distributed characteristics such as superheat response. This model relates the dynamic responses of several critical variables such as evaporating temperature and the refrigerant superheat at the heat exchanger outlet, to changes in boundary conditions, including the inflow and outflow rates as well as the inflow enthalpy. This model of two-phase flow heat exchanger is essential for the establish of a lumped-parameter model of vapor compression cycles.

A new model of vapor compression cycles

A lumped-parameter model for describing the dynamics of a vapor compression cycle has been presented. One of the main features of this model is in its effective characterization of superheat response, in addition to pressure response, to actuator inputs. Although superheat regulation is highly essential in a vapor compression cycle, its dynamic characteristics has never been captured by any previous model which is con-

cise enough to incorporate into control design. This model, expressed explicitly in a transfer function matrix, is highly useful for designing control systems that coordinate several actuator inputs so as to achieve capacity modulation and superheat regulation simultaneously.

MIMO control of vapor compression cycles based on the dynamic model

Multivariable feedback control has been proposed to regulate a vapor compression cycle based on the proposed lumped-parameter model. The conventional SISO method of controlling a vapor compression cycle was shown to have very limited performance. The LQG technique has been applied to synthesize a model-based multivariable control system with guaranteed stability robustness in the design. To control a vapor compression cycle over a wide range where system nonlinearities become evident, the multivariable controller has been designed to adapt to changing operating conditions based on a gain scheduling scheme. The multivariable control was analytically and experimentally demonstrated to have much better performance than the conventional SISO method. This thesis is the first attempt to utilize a dynamic model to design MIMO control for vapor compression refrigeration systems.

5.2 Main Impacts on HVAC&R Systems

This thesis has direct impacts on a variety of HVAC and refrigeration systems including air conditioners, heat pumps, and refrigerator etc. The following aspects illustrate the main impacts of this thesis on HVAC&R Systems.

Controlling superheat at a lower value to increase energy efficiency

The evaporating efficiency is largely dependent on the value of superheat. A high superheat value implies a longer superheated section which has much smaller heat transfer coefficient than the two-phase section in an evaporator. The higher the su-

perheat value, the lower the energy efficiency. Ideally, with a zero superheat, the system has highest energy-efficiency. However, a positive superheat value much be maintained to prevent liquid refrigerant from entering the compressor. With conventional control schemes (thermostatic expansion valve or any PID control of electronic expansion valve), the desired value of superheat has to be set relatively high, due to the limited stability and efficacy of SISO control. It was demonstrated in the thesis that MIMO control techniques can take advantage of cross couplings in vapor compression systems to better and effectively regulate superheat response by properly coordinating the compressor speed and valve opening. This manifests that the desired value of superheat can be set relatively low in the systems with MIMO control. Therefore the overall system energy-efficiency can be increased.

Quick and stable response to indoor temperature setting change

Change of indoor temperature setting is often made due to reasons such as uncomfortable thermal sensation. We expect a quick response of the air conditioner that can change the indoor air temperature to the new setting for the desired thermal comfort. As shown in the thesis, multivariable control can quickly respond to the setting change without causing instability of the system. Instability of the system may occur if quick action is taken based on a conventional control.

Integrating with set-point optimization to achieve high energy efficiency

In addition to variable-speed compressors and adjustable electronic expansion valve, variable-speed indoor and outdoor fans are becoming available in heat pumps and air conditioners now. There exist multiple combinations of compressor speed, indoor fan speed, outdoor fan speed, and expansion valve opening that can satisfy cooling (or heating) load condition or thermal comfort requirement. However, the most energy-efficient operation where the COP is maximized corresponds to a certain combination

of these control inputs, i.e. the optimal set-point. If the optimal set-point can be determined and stablized under arbitrary indoor and outdoor environment, these modern variable-speed drives can be exploited to significantly improve the energy efficiency of vapor compression systems. The multivariable control discussed in the thesis can stablize an optimal set-point or realize fast and stable transitions between changing optimal set-points under changing outdoor temperature.

Potential for more complicated systems

There are many more complicated HVAC systems than residential air conditioners. Several examples are multi-systems which have more than one indoor heat exchanger, and big building HVAC systems which include many integrated components. Such complicated systems possess many actuators like compressors, fans, and valves. These actuators usually need to be operated to achieve multi-goals. Decoupled control system generally result in either low energy-efficiency or low performance to achieve these multi-goals. It is more beneficial to develop multivariable control for those complicated systems. The framework proposed in this thesis could be useful for developing advanced control in many more complicated HVAC systems.

References

[1] Anonymous, "Innovative air conditioning and refrigeration research: meeting global opportunities", *The Air Conditioning and Refrigeration Institute Report*, December, 1993.

[2] Broersen, P. M. T. and van der Jagt, M. T. G., "Hunting of evaporators controlled by a thermostatic expansion valve", *ASME J. Dynamic Systems, Measurement, and Control*, Vol. 102, June 1980.

[3] Chi, J. and Didion, D., "A simulation of the transient performance of a heat pump", *Int. J. Refrigeration*, Vol.5, No.3, pp. 176-184, 1982.

[4] Den Braven, K., Herold, K., Mei, V., O'Neal, D., and Penoncello, S., "Imporving heat pumps and air conditioning", *ASME Mechanical Engineering*, Vol. 115, September, 1993, pp. 98-102.

[5] Dhar, M. and Soedel, W., "Transient analysis of a vapor compression refrigeration system", *Proc. 25th Int. Cong. of Refrigeration*, Venice, Italy, 1979.

[6] Domanski, P. and Didion, D., "Computer modeling of the vapor compression cycle with constant flow area expansion device", *National Bureau of Standard*, PB83-226639, 1983.

[7] Fanger, P.O., *Thermal Comfort*, McGraw-Hill, 1970

[8] Federspiel, C.C., User-Adaptable and Minimum-Power Thermal Comfort Control, Ph.D. Thesis, Massachusetts Institute of Technology, 1992

[9] Grald, E.W. and MacArthur, J.W., "A moving-boundary formulation for modeling time-dependent two-phase flows", *Int. J. Heat and Fluid Flow*, Vol. 13, No. 3, pp. 266 - 272, 1992.

[10] Gruhle, W.-D. and Isermann, R., "Modeling and control of a refrigerant evaporator", *ASME J. Dynamic Systems, Measurement, and Control*, Vol. 107, pp. 235-239, December, 1985.

[11] Gyftopoulos, E.P. and Berette, G.P., Thermodynamics: Foundation and Applicatio ns, Macmillan Publishing Company, New York, 1991

[12] He, X., Liu, S., and Asada, H., "A moving-interface model of two-phase flow heat exchanger dynamics for control of vapor compression cycle", *Heat pump and refrigeration system design, analysis, and application*, K. R. Den Braven and V. Mei, ed., ASME AES-Vol. 32, pp. 69-75, 1994.

[13] He, X., Liu, S., and Asada, H., "Modeling of vapor compression cycles for advanced controls in HVAC systems", *Proceeding of American Control Conference*, Seattle, June, 1995.

[14] He, X., Liu, S., and Asada, H., "Multivariable Feedback Design for regulating vapor compression cycles", *Proceeding of American Control Conference*, Seattle, June, 1995.

[15] Hiller, C. C. and Glicksman, L. R., "Improving heat pump performance via compressor capacity control - analysis and test", *MIT Heat Transfer Laboratory*, Report No. 24525-96, 1976.

[16] Koudo, I., Miyake, I., and Suda, H., "Two-variable control of refrigeration cycle using electronic expansion valves and inverters", *1986 Japaness Refrigeration Conf.*, pp. 77-80, 1986.

[17] MacArthur, J.W., "Transient heat pump behavior: a theoretical investigation", *InT. J. Refrigeration*, Vol.7, No., pp. 123-132, 1984.

[18] MacArthur, J. W. and Grald, E. W., "Unsteady compressible two-phase flow model for predicting cyclic heat pump performance and a comparison with experimental data", *Int. J. Refrigeration*, Vol. 12, pp. 29-41, 1989.

[19] MacArthur, J.W. and Grald, E.W., "Prediction of cyclic heat pump performance with a fully distributive model and a comparison with experimental data", *ASHRAE Trans.*, Vol. 93, Part 2, 1987.

[20] MacArthur, J.W. and Grald, E.W.," Optimal comfort control for variable-speed heat pumps", *ASHRAE Transactions*, Vol. 94, Part 2, pp. 1283-1297, 1988

[21] MacArthur, J. W. and Grald, E. W., "Unsteady compressible two-phase flow model for predicting cyclic heat pump performance and a comparison with experimental data", *Int. J. Refrigeration*, Vol. 12, pp. 29-41, 1989.

[22] McQuiston, F. and Parker, J., *Heating, Ventilating, and Air Conditioning, Design and Analysis*, 4th edition, John Wiley pand Sons, 1994.

[23] Miller, W.A., "Steady-state refrigerant flow and airflow control experiments for a continuously variable speed air-to-air heat pump", *ASHRAE Transactions*, Vol. 93, pp. 1191-1204, 1987

[24] Palmer, Z., "Design of Advanced process controllers", *AIChE Journal*, Vol. 27, No. 5, pp. 793-805, 1981.

[25] Patankar, S.V., *Numerical Heat Transfer and Fluid Flow*, New York, McGraw-Hill, 1980.

[26] Proceedings of the Purdue Compressor Technology Conference, Purdue Research Foundation, 1978, 1980, 1982, 1984, 1986, 1988, 1990, 1992.

[27] Sami, S.M. et al, "Prediction of the transient response of heat pumps", *ASHRAE Trans.*, Vol. 93, Part 2, pp. 471-489, 1987.

[28] Shoureishi, R. and McLaughlin, K., "Modeling and dynamics of two-phase flow heat exchangers using temperature-entropy bond graphs", *Proc. 1984 American Control Conf.*, pp. 93-98, 1984.

[29] Wedekind, G. L. and Stoecker, W. F., "Transient response of the mixture-vapor transition point in horizontal evaporating flow", *ASHRAE Journal*, November, pp. 74 -77, 1966.

[30] Wedekind, G. L., Bhatt, B. L., and Beck, B. T., "A system mean void fraction model for predicting various transient phenomena associated with two-phase evaporating and condensing flows", *Int. J. Multiphase Flow*, Vol. 4, pp. 97-114, 1978.

[31] Yasuda, H. and Ishibane, H., "Analysis of evaporator superheat control using electronic expansion valves", *Proc. 1986 Japaness Refrigeration Conf.*, pp. 73-76, 1986.

Appendix A

Derivations of equations (2.9) and (2.10) are given as follows. The derivations involve integration with time-dependent limits of integration. The following integration equation is applied.

$$\int_{z_1(t)}^{z_2(t)} \frac{\partial f(z,t)}{\partial t} dz = \frac{d}{dt}\int_{z_1(t)}^{z_2(t)} f(z,t)dz - f(z_2(t),t)\frac{dz_2(t)}{dt} + f(z_1(t),t)\frac{dz_1(t)}{dt} \quad \text{(A1)}$$

Integration of the energy balance equation from $z = 0$ to $z = L_1(t)$ for the two-phase flow section gives rise to

$$A\int_0^{L_1(t)} \frac{\partial(\rho h)}{\partial t} dz - AL_1(t)\frac{dP(t)}{dt} = \dot{m}_i h_i - \dot{m}_{int} h_{int} + q_1 \quad \text{(A2)}$$

where

$$q_1 = \alpha_i \pi D_i L_1(t)(T_{w1}(t) - T_{r1})$$

Applying equation (A1), we have

$$\begin{aligned}
&\int_0^{L_1(t)} \frac{\partial(\rho h)}{\partial t} dz \\
&= \frac{d}{dt}\int_0^{L_1(t)} \rho h dz - \rho_g h_g \frac{dL_1(t)}{dt} \\
&= \frac{d}{dt}\int_0^{L_1(t)} (\rho_l h_l(1-\gamma) + \rho_g h_g \gamma) dz - \rho_g h_g \frac{dL_1(t)}{dt} \\
&= \frac{d}{dt}\left(\rho_l h_l \int_0^{L_1(t)} (1-\gamma)dz + \rho_g h_g \int_0^{L_1(t)} \gamma dz\right) - \rho_g h_g \frac{dL_1(t)}{dt} \\
&= \frac{d}{dt}\left(L_1(t)\rho_l h_l(1-\bar{\gamma}) + L_1(t)\rho_g h_g \bar{\gamma}\right) - \rho_g h_g \frac{dL_1(t)}{dt} \\
&= L_1(t)\left(\frac{d(\rho_l h_l)}{dt}(1-\bar{\gamma}) + \frac{d(\rho_g h_g)}{dt}\bar{\gamma}\right) + (1-\bar{\gamma})(\rho_l h_l - \rho_g h_g)\frac{dL_1}{dt} \quad \text{(A3)}
\end{aligned}$$

where γ is the void fraction defined as the volume fraction of vapor relative to the total volume of the two-phase mixture at any flow section. $\bar{\gamma}$ is the mean value of the void fraction which can be determined based on the density profile.

Integration of the mass balance equation from $z = 0$ to $z = L_1(t)$ gives

$$A\int_0^{L_1(t)} \frac{\partial \rho}{\partial t} = \dot{m}_i - \dot{m}_{int} \tag{A4}$$

$$\begin{aligned}
\int_0^{L_1(t)} \frac{\partial \rho}{\partial t} dz &= \frac{d}{dt}\int_0^{L_1(t)} (\rho_l(1-\gamma) + \rho_g\gamma)dz - \rho_g \frac{dL_1(t)}{dt} \\
&= \frac{d}{dt}\left(L_1(t)\frac{1}{L_1(t)}\int_0^{L_1(t)} (\rho_l(1-\gamma) + \rho_g\gamma)dz\right) - \rho_g \frac{dL_1(t)}{dt} \\
&= L_1(t)\frac{d\rho_1}{dP}\frac{dP(t)}{dt} + (\rho_1 - \rho_g)\frac{dL_1(t)}{dt}
\end{aligned} \tag{A5}$$

where $\rho_1 = \rho_l(1-\bar{\gamma}) + \rho_g\bar{\gamma}$.

The energy balance equations for the tube walls of two-phase flow section and one-phase flow can be obtained in a similar way.

Appendix B

Elements in matrices $\boldsymbol{D}$, $\boldsymbol{A}'$, and $\boldsymbol{B}'$ for the evaporator model are as follows.

$d_{11} = -A(1-\bar{\gamma})\rho_l h_{fg}$

$d_{12} = AL_1(-(1-\bar{\gamma})\frac{d(\rho_l h_{fg})}{dP} + \rho_1 \frac{dh_g}{dP} - \beta)$

$d_{21} = -\frac{1}{2}A(h_o - h_g)\rho_2$

$d_{22} = AL_2(0.5\rho_2 \frac{dh_g}{dP} + 0.5(h_o - h_g)\frac{\partial \rho_2}{\partial P} - \beta)$

$d_{23} = AL_2(0.5\rho_2 + 0.5(h_o - h_g)\frac{\partial \rho_2}{\partial h_o})$

$d_{31} = A(\rho_1 - \rho_2)$

$d_{32} = AL_1 \frac{d\rho_1}{dP} + AL_2 \frac{\partial \rho_2}{\partial P}$

$d_{33} = AL_2 \frac{\partial \rho_2}{\partial h_o}$

$d_{44} = (C_p \rho A)_w$

$d_{51} = (C_p \rho A)_w \frac{T_{w_1} - T_{w_2}}{L_2}$

$d_{55} = (C_p \rho A)_w$

$a'_{11} = \alpha_{i1}\pi D_i(T_{w_1} - T_{r1})$

$$a'_{12} = -\dot{m}_i \frac{dh_g}{dP} - \alpha_{i1}\pi D_i L_1 \frac{dT_{r1}}{dP}$$

$$a'_{14} = \alpha_{i1}\pi D_i L_1$$

$$a'_{21} = -\alpha_{i2}\pi D_i (T_{w_2} - T_{r2})$$

$$a'_{22} = \dot{m}_o \frac{dh_g}{dP} - \alpha_{i2}\pi D_i L_2 \frac{\partial T_{r2}}{\partial P}$$

$$a'_{23} = -\dot{m}_o - \alpha_{i2}\pi D_i L_2 \frac{\partial T_{r2}}{\partial h_o}$$

$$a'_{25} = \alpha_{i2}\pi D_i L_2$$

$$a'_{42} = \alpha_{i1}\pi D_i \frac{dT_{r1}}{dP}$$

$$a'_{44} = -(\alpha_{i1}\pi D_i + \alpha_{o2}\pi D_o)$$

$$a'_{52} = \alpha_{i2}\pi D_i \frac{\partial T_{r2}}{\partial P}$$

$$a'_{53} = \alpha_{i2}\pi D_i \frac{\partial T_{r2}}{\partial h_o}$$

$$a'_{55} = -(\alpha_{i2}\pi D_i + \alpha_{o2}\pi D_o)$$

$$b'_{11} = h_i - h_g$$

$$b'_{12} = \dot{m}_i$$

$$b'_{23} = h_g - h_o$$

$$b'_{44} = \pi D_o (T_a - T_{w_1}) \frac{d\alpha_{o1}}{dv_a}$$

$$b'_{54} = \pi D_o (T_a - T_{w_2}) \frac{d\alpha_{o2}}{dv_a}$$

Appendix C

In this appendix, the detailed derivations of equations (3.6) and (3.8) are given. Integration of the energy balance equation from $z = L_1(t)$ to $z = L_2(t)$ for the two-phase flow section in a condenser gives rise to

$$A \int_{L_1(t)}^{L_1(t)+L_2(t)} \frac{\partial(\rho h)}{\partial t} dz - AL_2(t) \frac{dP(t)}{dt} = \dot{m}_{int1} h_g - \dot{m}_{int2} h_l + q_2 \qquad \text{(C1)}$$

where

$$q_2 = \alpha_{i2}\pi D_i L_2(t)(T_{w2} - T_{r2})$$

Applying equation (A1), we have

$$\begin{aligned}
&\int_{L_1(t)}^{L_1(t)+L_2(t)} \frac{\partial(\rho h)}{\partial t} dz \\
&= \frac{d}{dt}\left[L_2 \frac{1}{L_2} \int_{L_1(t)}^{L_1(t)+L_2(t)} \rho h dz\right] - \rho_l h_l \frac{d(L_1(t)+L_2(t))}{dt} + \rho_g h_g \frac{dL_1(t)}{dt} \\
&= \frac{d}{dt}\left[L_2(\rho_l h_l(1-\bar{\gamma}) + \rho_g h_g \bar{\gamma})\right] - \rho_l h_l \frac{d(L_1(t)+L_2(t))}{dt} + \rho_g h_g \frac{dL_1(t)}{dt} \\
&= L_2\left(\frac{d(\rho_l h_l)}{dt}(1-\bar{\gamma}) + \frac{d(\rho_g h_g)}{dt}\bar{\gamma}\right) + (\rho_g h_g - \rho_l h_l)\frac{dL_1}{dt} + \bar{\gamma}(\rho_g h_g - \rho_l h_l)\frac{dL_2}{dt} \qquad \text{(C2)}
\end{aligned}$$

where γ is the void fraction defined as the volume fraction of vapor relative to the total volume of the two-phase mixture at any flow section. $\bar{\gamma}$ is the mean value of the void fraction which can be determined based on the density profile.

Integration of the mass balance equation from $z = L_1(t)$ to $z = L_2(t)$ gives

$$A \int_{L_1(t)}^{L_1(t)+L_2(t)} \frac{\partial \rho}{\partial t} dz = \dot{m}_{int1} - \dot{m}_{int2} \qquad \text{(C3)}$$

$$\begin{aligned}
\int_{L_1(t)}^{L_1(t)+L_2(t)} \frac{\partial \rho}{\partial t} dz &= \frac{d}{dt}\left[L_2 \frac{1}{L_2} \int_{L_1(t)}^{L_1(t)+L_2(t)} \rho dz\right] - \rho_l\left(\frac{dL_1(t)}{dt} + \frac{dL_2(t)}{dt}\right) + \rho_g \frac{dL_1(t)}{dt} \\
&= \frac{d}{dt}(L_2\rho_2) - \rho_l\left(\frac{dL_1(t)}{dt} + \frac{dL_2(t)}{dt}\right) + \rho_g \frac{dL_1(t)}{dt} \\
&= L_2 \frac{d\rho_2}{dt} + (\rho_g - \rho_l)\frac{dL_1}{dt} + (\rho_2 - \rho_l)\frac{dL_2}{dt} \qquad \text{(C4)}
\end{aligned}$$

where $\rho_2 = \rho_l(1-\bar{\gamma}) + \rho_g\bar{\gamma}$.

Appendix D

Elements in matrices $\boldsymbol{D}$, $\boldsymbol{A'}$, and $\boldsymbol{B'}$ for the condenser model are as follows.

$d'_{11} = 0.5A\rho_1(h_i - h_g)$

$d'_{13} = AL_1(\rho_1 dh_g/dP + 0.5(h_i - h_g)(d\rho_1/dP + d\rho_1/dh_1 dh_g/dP) - \beta)$

$d'_{21} = A\rho_l h_{fg}$

$d'_{22} = A\bar{\gamma}\rho_l h_{fg}$

$$d'_{23} = AL_2(-(1-\bar{\gamma})d(\rho_l h_{fg})/dP + \rho_2 dh_g/dP - \beta)$$

$$d'_{31} = A\rho_l 0.5(h_l - h_o)$$

$$d'_{32} = A\rho_l 0.5(h_l - h_o)$$

$$d'_{33} = AL_3(0.5\rho_l dh_l/dP - \beta)$$

$$d'_{34} = 0.5AL_3\rho_l$$

$$d'_{41} = A(\rho_1 - \rho_l)$$

$$d'_{42} = A(\rho_2 - \rho_l)$$

$$d'_{43} = AL_1(d\rho_1/dP + d\rho_1/dh_1 dh_g/dP) + AL_2 d\rho_2/dP$$

$$d'_{51} = (C_P\rho A)_w(T_{w1} - T_{w2})/L_1$$

$$d'_{55} = (C_P\rho A)_w$$

$$d'_{66} = (C_P\rho A)_w$$

$$d'_{71} = (C_P\rho A)_w(T_{w2} - T_{w3})/L_3$$

$$d'_{72} = (C_P\rho A)_w(T_{w2} - T_{w3})/L_3$$

$$d'_{77} = (C_P\rho A)_w$$

$$a'_{11} = \alpha_{i1}\pi D_i(T_{w1} - T_{r1})$$

$$a'_{13} = -(m_i dh_g/dP + \alpha_{i1}\pi D_i L_1(dT_{r1}/dP + dT_{r1}/dh_1 dhg/dP))$$

$$a'_{15} = \alpha_{i1}\pi D_i L_1$$

$$a'_{22} = \alpha_{i2}\pi D_i(T_{w2} - T_{r2})$$

$$a'_{23} = m_o dh_g/dP - m_o dh_l/dP - \alpha_{i2}\pi D_i L_2 dT_{r2}/dP$$

$$a'_{26} = \alpha_{i2}\pi D_i L_2$$

$$a'_{31} = -\alpha_{i3}\pi D_i(T_{w3} - T_{r3})$$

$$a'_{32} = -\alpha_{i3}\pi D_i(T_{w3} - T_{r3})$$

$$a'_{33} = m_o dh_l/dP - \alpha_{i3}\pi D_i L_3 dT_{r3}/dP$$

$$a'_{34} = -m_o - \alpha_{i3}\pi D_i L_3 dT_{r3}/dh_o$$

$$a'_{37} = \alpha_{i3}\pi D_i L_3$$

$$a'_{53} = \alpha_{i1}\pi D_i(dT_{r1}/dP + dT_{r1}/dh_1 dhg/dP)$$

$$a'_{55} = -(\alpha_{i1}\pi D_i + \alpha_o \pi D_o)$$

$$a'_{63} = \alpha_{i2}\pi D_i dT_{r2}/dP$$

$$a'_{66} = -(\alpha_{i2}\pi D_i + \alpha_o \pi D_o)$$

$$a'_{73} = \alpha_{i3}\pi D_i dT_{r3}/dP$$

$$a'_{74} = \alpha_{i3}\pi D_i dT_{r3}/dh_o$$

$$a'_{77} = -(\alpha_{i3}\pi D_i + \alpha_o \pi D_o)$$

$$b'_{11} = h_i - h_g$$

$$b'_{12} = m_i$$

$$b'_{23} = h_g - h_l$$

$$b'_{33} = h_l - h_o$$

$$b'_{54} = \pi D_o(T_a - T_{w1})\frac{d\alpha_{o1}}{dv_c}$$

$$b'_{64} = \pi D_o(T_a - T_{w2})\frac{d\alpha_{o2}}{dv_c}$$

$$b'_{74} = \pi D_o(T_a - T_{w3})\frac{d\alpha_{o3}}{dv_c}$$

Expressions for k'_{ij} are as follows.

$$k'_{11} = -\frac{\dot{m}_1}{2(P_c^s - P_e^s)} \qquad k'_{12} = \frac{\dot{m}_1}{2(P_c^s - P_e^s)} \qquad k'_{13} = \frac{\dot{m}_1}{A_v^s}$$

$$k'_{21} = \frac{\frac{\partial h_{3s}}{\partial P_e}}{\eta_c} \qquad k'_{22} = \frac{\frac{\partial h_{3s}}{\partial P_c}}{\eta_c} \qquad k'_{23} = \left(\frac{\partial h_{3s}}{\partial h_2} - 1\right)/\eta_c + 1$$

$$k'_{31} = \frac{\partial f(\frac{P_c}{P_e}, u_1)}{\partial P_e} \qquad k'_{32} = \frac{\partial f(\frac{P_c}{P_e}, u_1)}{\partial P_c} \qquad k'_{33} = \frac{\partial f(\frac{P_c}{P_e}, u_1)}{\partial u_1}$$

For a reciprocating compressor,

$$k'_{31} = \frac{P_c}{P_e^2}\left(\frac{\dot{m}_2 C_c(\frac{P_c}{P_e})^{1/n-1}\frac{1}{n}}{1 + C_c - C_c(\frac{P_c}{P_e})^{1/n}}\right) \qquad k'_{32} = -\frac{1}{P_e}\left(\frac{\dot{m}_2 C_c(\frac{P_c}{P_e})^{1/n-1}\frac{1}{n}}{1 + C_c - C_c(\frac{P_c}{P_e})^{1/n}}\right) \qquad k'_{33} = \frac{\dot{m}_2}{\omega^s}$$